TR

A Geometric Analysis of Stability Regions for a Linear Differential Equation with Two Delays

Joseph M. Mahaffy *
Department of Mathematical Sciences
San Diego State University
San Diego, CA 92182-0314.

Paul J. Zak †
Department of Economics
University of Pennsylvania
Philadelphia, PA 19104-6297.

Kathryn M. Joiner ‡
Department of Mathematical Sciences
San Diego State University
San Diego, CA 92182-0314.

December 28, 1992

*The work of this author was supported in part by NSF grant DMS-8807360 and DMS-9007718.

†The work of this author was supported under the REU program of NSF by grant DMS-8807360 and by the University of Pennsylvania.

‡The work of this author was supported under the REU program of NSF by grant DMS-9007718. She currently resides in Kirkland, WA.

Abstract

A geometric approach is used to determine the region of stability for a linear differential equation with two delays. The imaginary and zero solutions of the charateristic equation produce an infinite set of surfaces in the coefficient parameter space. A methodology is outlined for identifying which of these surfaces comprise the boundary of the stability region. For a range of delays, the stability region changes in only three ways, starting at an identified initial point and becoming more complex as one coefficient increases. Detailed graphical analyses, including three-dimensional plots, show the evolution of the stability surface for given ratios of delays, highlighting variations across delays. The results demonstrate that small changes in the delay ratio cause signficant changes in the size and shape of the stability region. An asymptotic analysis of the stability region shows that certain rational delay ratios have atypically large regions of stability compared to nearby delays.

1 Introduction

Models using delay differential equations have appeared with increasing frequency in a variety of applications (e.g., [2, 3, 4, 5, 13, 15, 16]). Considerable work has been done on the analysis of differential equations with one delay; however, much less is known about stability for multiple delay problems. This work identifies some of the difficulties in analyzing a differential equation with two delays and provides a systematic scheme for determining the region of stability. Our approach is based on a geometric analysis of the characteristic equation for a differential equation with two delays.

This work considers a scalar linear first order differential equation with two delays. The general form of this equation is:

$$y'(t) + ay(t) + by(t - r_1) + cy(t - r_2) = 0. \tag{1.1}$$

The stability of (1.1) depends on its five parameters and can be determined by locating the complex roots of the associated characteristic equation:

$$\lambda + a + be^{-r_1\lambda} + ce^{-r_2\lambda} = 0. \tag{1.2}$$

The zero solution of (1.1) is asymptotically stable if all roots of (1.2) have negative real parts. Since this characteristic equation is an exponential polynomial with two different exponential functions in the eigenvalues, λ, the analysis is particularly difficult. Furthermore, the five-dimensional parameter space makes geometric interpretation of the stability region impossible in general. A scaling of either y or t can be used to eliminate one parameter, but this still leaves a four-dimensional parameter space to consider.

Techniques that locate the roots of (1.2) have been investigated in a number of special cases. The one delay problem ($c = 0$) has been completely solved by Hayes [12]. Several authors [17, 18] have considered the case when $a = 0$ and $r_1 = 1$ with other specific restrictions. Other authors [8, 14] have examined extensions of this problem to determine when oscillations occur by showing the existence of complex roots of the characteristic equation, though stability is not directly addressed. More recently, there have been several papers which have performed a more complete analysis of (1.1) [1, 4, 5, 19]. Most of these have been attempts to characterize the stability region of the four parameter problem using two dimensional projections in the parameter space. An alternative approach is taken by Hale and Huang [11] who give a geometrical description of the stability for (1.1) in the r_1r_2-parameter space. Finding regions in the parameter space where the solutions of (1.1)

are asymptotically stable is recognized as a difficult problem [1, 6, 11, 9, 12, 17, 19].

This paper examines the stability of (1.1) after one of the delays has been normalized by a rescaling of time. The analysis considers a range of values for the second delay and systematically constructs the complete stability surface in the coefficient parameter space as the coefficient, a, of the undelayed term in (1.1) is increased. The solutions of the characteristic equation (1.2) with purely imaginary or zero roots form an infinite set of surfaces in the coefficient parameter space. The boundary of the stability region is a surface created from intersecting portions of this infinite set of surfaces. At this boundary either Hopf bifurcations at various frequencies occur or there is a zero root crossing. Section 3 provides the basic definitions and theorems that are used to describe the evolution of the stability surface. For a given delay, the stability surface comes to a point at some minimum value of a, then as a increases the stability surface becomes more complex as higher frequency Hopf bifurcations affect the boundary of the stability region. However, there are only three ways that new bifurcation surfaces enter the boundary of the stability region, yielding discernable patterns in its construction. Three-dimensional graphics illustrate the complete stability surfaces for several values of the second delay.

A theorem is provided that establishes a minimum region of stability independent of the delays in the coefficient parameter space. Our analysis determines how much the actual stability region exceeds this minimum stability region for a given delay. Section 4 details the evolution of the stability surface when the second delay is $\frac{1}{3}$, showing the complexity of the stability surface. For example, a small region of stability appears to be disconnected from the principal stability region in bc-cross-sections, but connectivity of the complete stability surface is maintained in the 3-dimensional structure. In addition, we identify particular values of a where the stability surface extends well beyond the minimum region of stability. This analysis is generalized in Section 5 to show that small changes in the delay can cause considerable changes in the stability surface. Section 6 contains a map for constructing the stability surface over a range of values for the second delay.

In Section 7, numerical methods are used to examine the asymptotic behavior of the stability region. Some special cases are bounded away from the minimum region of stability, while most delays result in an asymptotic approach to the minimum stability region. Our geometric analysis suggests that certain ordering properties in the infinite set of curves generated by (1.2) may prevent the region of stability from asymptotically approaching

the minimum region of stability when r_2/r_1 is rational. This indicates the sensitivities inherent in mathematical models using differential equations with two delays. In particular, researchers frequently test their models using the ratio of delays $r_2/r_1 = \frac{1}{2}$, for which the region of stability is shown to be 68% larger than the minimum region of stability.

The ideas of this paper were first presented at a conference at the Claremont Colleges in honor of Kenneth Cooke in January 1990. The long delay in producing this paper is due to the geometric nature of the project and complicated nature of differential equations with two delays.

2 Stability of the One Delay Problem

In this section we review the stability analysis of a scalar linear first order differential equation with one delay. The most general form is given by (1.1) with $c = 0$. By rescaling time ($\tau = t/r_1$), this delay differential equation can be written:

$$\dot{y}(\tau) + Ay(\tau) + By(\tau - 1) = 0, \tag{2.1}$$

where $A = r_1 a$ and $B = r_1 b$. If $\phi(\tau)$ is a continuous function defined for $\tau \in [-1, 0]$ and $y(\tau) = \phi(\tau)$ for $\tau \in [-1, 0]$, then there exists a unique, continuously differentiable solution, $y(\tau)$, to (2.1) for all $\tau > 0$ [10].

Eqn. (2.1) has the unique equilibrium solution, $y(\tau) \equiv 0$ for all τ. Stability of the trivial solution is found by analyzing the characteristic equation for (2.1) which is given by:

$$\lambda + A + Be^{-\lambda} = 0. \tag{2.2}$$

As noted before, the asymptotic stability of (2.1) is equivalent to all solutions, λ, of (2.2) having real parts less than zero. Thus, we can divide the AB-plane into regions where all solutions of (2.2) have negative real parts so that (2.1) is asymptotically stable, and regions where there is at least one root with Re $\lambda \geq 0$. From stability analysis of ordinary differential equations it is clear that the positive A-axis is part of the region of asymptotic stability.

Hale ([10], pp. 168) shows that the spectrum or eigenvalues of (2.1) have their real parts bounded above. This implies that if one locates the eigenvalues with maximum real part, then they can be used to determine the stability of the system. Continuous dependence of the roots of (2.2) on

the parameters A and B indicates that the boundary of the stability set for (2.1) is a subset of the mapping of the imaginary axis in the λ-plane into the AB-plane. For $\lambda = 0$, which is where a real root crosses the imaginary axis, (2.2) is satisfied whenever $A+B = 0$. By connectedness of the stability region [7], this implies that the region of stability is a subset of the half-plane $A + B > 0$.

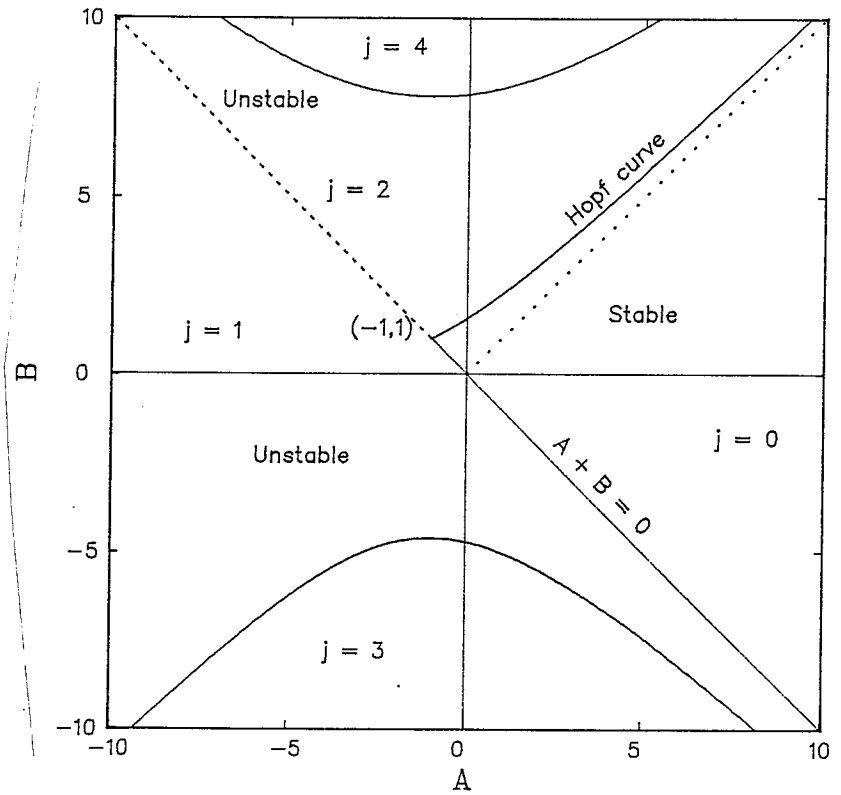

Figure 2.1: Region of stability and bifurcation curve for the one delay problem. The j values show how many eigenvalues have positive real parts.

The remainder of the boundary of the stability set is found by locating where Hopf bifurcations occur (*i.e.*, when a pair of eigenvalues cross the imaginary axis). The critical eigenvalues are found by letting $\lambda = i\omega$. This substitution in (2.2) yields:

$$i\omega + A + B(\cos\omega - i\sin\omega) = 0,$$

or equivalently,

$$\begin{aligned} A &= -B\cos\omega, \\ B &= \frac{\omega}{\sin\omega}. \end{aligned} \tag{2.3}$$

The equations (2.3) are parametrized by ω and are defined on each interval $k\pi < \omega < (k+1)\pi$, $k = \ldots, -1, 0, 1, \ldots$ It is readily shown that

$$\lim_{\omega\to 0} B = 1 = -\lim_{\omega\to 0} A,$$

so the first bifurcation curve begins at the point $(-1, 1)$ in the AB-plane. As

$$\lim_{\omega\to\pi^-} B = +\infty = \lim_{\omega\to\pi^-} A,$$

it can be seen that this curve asymptotically approaches the line $A = B$ as $\omega \to \pi^-$. This provides the other boundary for the stability set of (2.1). Additional bifurcation curves represent locations where higher frequency roots cross the imaginary axis, all of which lie outside the region bounded by the first bifurcation curve and the half line with $A = -B$, $A \geq -1$. Fig. 2.1 shows the region of stability and includes the images of (2.3) with $2\pi < \omega < 3\pi$ and $3\pi < \omega < 4\pi$, which lie completely outside the region of stability. In Fig. 2.1, the number of roots of the characteristic equation (2.2) with positive real part is given by j. More discussion of how j is determined is given in Section 4.

If the rescaling is not done to (1.1), then stability region for the one delay problem with $c = 0$ can be found in a similar manner to the one described above for (2.1). The shape of the stability region is the same with the Hopf bifurcation curve intersecting the line $a = -b$ at the point $(-\frac{1}{r_1}, \frac{1}{r_1})$. The parameterization of the Hopf bifurcation curve ranges over the interval $0 < \omega < \frac{\pi}{r_1}$. Consequently, the stability region and the interval of ω increase as r_1 decreases. This information is valuable in examining the cross-section of the stability region for the two delay problem when the coefficient of the normalized delay is zero.

3 Tools and Techniques for Analysis of the Two Delay Problem

A typical scalar linear first order differential equation with two delays is given by (1.1). Without loss of generality, one can assume that $r_1 > r_2$, so

the same rescaling of time as presented in the previous section reduces (1.1) into the four parameter problem:

$$\dot{y}(\tau) + Ay(\tau) + By(\tau - 1) + Cy(\tau - R) = 0, \quad 0 < R < 1, \tag{3.1}$$

where $A = r_1 a$, $B = r_1 b$, $C = r_1 c$, and $R = r_2/r_1$. As before, if $\phi(\tau)$ is a continuous function defined for $\tau \in [-1, 0]$ and $y(\tau) = \phi(\tau)$, then there exists a unique, continuously differentiable solution, $y(\tau)$, to (3.1) for all $\tau > 0$.

The trivial solution, $y(\tau) \equiv 0$, is the unique equilibrium solution to (3.1). The characteristic equation, which is used to analyze the stability of the equilibrium solution, is given by:

$$\lambda + A + Be^{-\lambda} + Ce^{-\lambda R} = 0. \tag{3.2}$$

There are four parameters to consider in the analysis of (3.2). This study examines the stability region in the three-dimensional space of the parameters A, B, and C for fixed values of R. The analytical approach we take in locating the stability region parallels Bélair [1] and Zaron [19], who use the D-decomposition partitions of El'sgol'ts [7]. (See Appendix A for more details.)

As in the one delay case, our graphical analysis shows that the stability region is a connected set in the ABC-parameter space for $R \in (0, \frac{1}{2}]$ though certain BC-cross-sections have disjoint regions of stability. We predict that the 3-dimensional stability region is connected for all $0 < R < 1$. Clearly, the positive half-line $A > 0$ must lie within the stability region. The results for (3.1) must be consistent with the one delay case, so Fig. 2.1 shows the cross-section of the stability region when $C = 0$ (and with rescaling resembles the cross-section for $B = 0$). How do the stability properties of (3.1) extend to the entire ABC-parameter space? A partial answer is provided by the following theorem:

THEOREM 3.1 (MINIMUM REGION OF STABILITY). *For $A > |B| + |C|$, all solutions, λ, to* (3.2) *have* Re $\lambda < 0$. *Thus, the differential equation* (3.1) *is asymptotically stable inside the pyramidal shaped region centered about the positive A-axis independent of R.*

The proof of this theorem can be found in Zaron [19].

The above result provides a *Minimum Region of Stability* (MRS). However, questions remain regarding how much larger the region of stability is

for (3.1) and how this region varies with R. As in the previous section, the search for the boundary of the region focuses on the image of the imaginary axis in the λ-plane. When $\lambda = 0$, any point on the plane $A+B+C = 0$ satisfies (3.2). This plane separates the ABC-parameter space into two parts where the region with $A+B+C < 0$ is unstable as it contains a unique real positive root. Since the plane $A + B + C = 0$ bounds one face of the MRS given in Theorem 3.1, one part of the stability region is comprised of this real root crossing surface. The remaining surfaces bounding the stability region are generated by examining the imaginary roots, $\lambda = i\omega$, where Hopf bifurcations occur. The remainder of this section is devoted to developing the tools needed to describe the geometry of the complete 3-dimensional stability surface. The following section has an illustrative example with figures that show how these tools are applied.

The next step of the analysis is to determine the image of the imaginary axis in the ABC-parameter space. If $\lambda = i\omega$, then (3.2) can be written:

$$A + B\cos(\omega) + C\cos(\omega R) + i(\omega - B\sin(\omega) - C\sin(\omega R)) = 0. \tag{3.3}$$

By splitting this into its real and imaginary parts and solving for B and C, we obtain the following parametric equations:

$$\begin{aligned} B(\omega) &= \frac{A\sin(\omega R) + \omega\cos(\omega R)}{\sin(\omega(1-R))}, \\ C(\omega) &= -\frac{A\sin(\omega) + \omega\cos(\omega)}{\sin(\omega(1-R))}. \end{aligned} \tag{3.4}$$

These equations are defined on the intervals, $\frac{(j-1)\pi}{1-R} < \omega < \frac{j\pi}{1-R}$, j an integer. As A varies with $\omega \in (\frac{(j-1)\pi}{1-R}, \frac{j\pi}{1-R})$, (3.4) generates a surface in the ABC-parameter space. For fixed A, (3.4) produces cross-sectional curves where the eigenvalues of (3.2) cross the imaginary axis in the BC-plane. Given this information we make the following definition:

DEFINITION. *The j^{th} bifurcation surface (curve) is the surface (curve) generated by the parametric equations* (3.4) *with $\frac{(j-1)\pi}{1-R} < \omega < \frac{j\pi}{1-R}$, where j is a positive integer.*

When the delay R is rational, the curves generated by (3.4) can be organized into families of bifurcation curves that possess similar properties. For certain values of the delay there are only a small number of families, which facilitates the analysis required to locate the boundary of the stability

region. Other delays that have larger numbers of families can be reorganized and compared to delays with only a small number of families. The method used to find families of bifurcation curves follows from the calculations below.

For A fixed, take $R = \frac{k}{n}$ and $j = n - k$. From (3.4), it is easy to see that singularities occur at $\frac{ni\pi}{j}$, $i = 0, 1, ...$ The i^{th} bifurcation surface with $\frac{n(i-1)\pi}{j} < \omega < \frac{ni\pi}{j}$ satisfies:

$$B_i(\omega) = \frac{A\sin(\frac{k\omega}{n}) + \omega\cos(\frac{k\omega}{n})}{\sin(\frac{j\omega}{n})}, \qquad C_i(\omega) = -\frac{A\sin(\omega) + \omega\cos(\omega)}{\sin(\frac{j\omega}{n})}.$$

Now consider the $(i + 2j)^{\text{th}}$ bifurcation surface with $\mu = \omega + 2n\pi$, then

$$\begin{aligned} B_{i+2j}(\mu) &= \frac{A\sin(\frac{k\mu}{n}) + \mu\cos(\frac{k\mu}{n})}{\sin(\frac{j\mu}{n})} = \frac{A\sin(\frac{k\omega}{n}) + (\omega + 2n\pi)\cos(\frac{k\omega}{n})}{\sin(\frac{j\omega}{n})}, \\ C_{i+2j}(\mu) &= -\frac{A\sin(\omega) + (\omega + 2n\pi)\cos(\omega)}{\sin(\frac{j\omega}{n})}. \end{aligned}$$

These equations show that $B_{i+2j}(\mu)$ follows the same trajectory as $B_i(\omega)$ with a shift of $2n\pi\cos(\frac{k\omega}{n})/\sin(\frac{j\omega}{n})$ for $\omega \in (\frac{(j-1)\pi}{1-R}, \frac{j\pi}{1-R})$, while $C_{i+2j}(\mu)$ follows the trajectory of $C_i(\omega)$ with a shift of $2n\pi\cos(\omega)/\sin(\frac{j\omega}{n})$ over the same values of ω. This related behavior of bifurcation surfaces separated by $\omega = 2n\pi$ creates $2j$ families of curves in the BC-plane for fixed A. Thus, there is a quasi-periodicity among the bifurcation surfaces when R is rational. In particular, when $R = \frac{1}{2}$ there are only two families of curves in the BC-plane. For $R = \frac{1}{3}$ and $R = \frac{1}{4}$, there are four and six families of curves in the BC-plane, respectively. In the next section, the case $R = \frac{1}{3}$ is examined in detail as the special features of this delay, including the limited number of families of bifurcation curves, simplify the geometric analysis of its stability region. The organization of the bifurcation curves into families appears to be especially significant in the asymptotic structure of the stability region as A becomes large. This is discussed in Section 7.

Fig. 2.1 shows that stability region for the one delay problem is completely determined by the first bifurcation curve and the line $A = -B$. For the two delay problem (3.1), the first bifurcation surface and the plane $A + B + C = 0$ do not necessarily give the complete stability picture. However, the first bifurcation surface can be used to bound the stability region and provides valuable information on how to begin the study of the stability surface for $R \in (R_0, \frac{1}{2}]$, where $R_0 \simeq 0.0117$ is defined in Appendix B. The

first bifurcation surface intersects the $A+B+C=0$ plane as $\omega \to 0$. From (3.4), this occurs when $B=(AR+1)/(1-R)$ and $C=-(A+1)/(1-R)$, which is the line

$$\frac{A+1}{1-R} = \frac{B-1}{R} = -C, \tag{3.5}$$

in the ABC-parameter space.

For some range of A values with ω increasing from zero, the first bifurcation surface intersects the $A+B+C=0$ plane a second time forming a curve in BC-space. As A decreases this curve intersects the line (3.5) at A_0, and the initial point from which the principal stability surface emanates is determined. For $R > R_0$, this initial point is the smallest value of A for which (3.1) is stable. When $R < R_0$, our studies show the existence of another region of stability for $A < A_0$. This issue is discussed in Appendix B. The following theorem summarizes our results:

THEOREM 3.2. *If $R > R_0$ and $A < -(R+1)/R$, then* (3.1) *is unstable independent of B and C. Geometrically, the stability surface comes to a point at*

$$(A_0, B_0, C_0) = \left(-\frac{R+1}{R},\ \frac{R}{R-1},\ \frac{1}{R(1-R)}\right), \tag{3.6}$$

and for some range of $A > A_0$, the stability region is bounded by the first bifurcation surface and the $A+B+C=0$ plane.

PROOF. Substituting (3.4) into the equation $A+B+C=0$, we find

$$A + \frac{A\sin(\omega R)+\omega\cos(\omega R)}{\sin(\omega(1-R))} - \frac{A\sin(\omega)+\omega\cos(\omega)}{\sin(\omega(1-R))} = 0.$$

This is solved for A giving,

$$\begin{aligned} A(\omega) &= \frac{\omega\left(\cos(\omega)-\cos(\omega R)\right)}{\sin(\omega(1-R))+\sin(\omega R)-\sin(\omega)}, \\ &= -\frac{\omega\sin\left(\frac{\omega(1+R)}{2}\right)}{2\sin\left(\frac{\omega}{2}\right)\sin\left(\frac{\omega R}{2}\right)}, \end{aligned} \tag{3.7}$$

provided $\sin(\omega(1-R)) \neq 0$ and $\sin\left(\frac{\omega(1-R)}{2}\right) \neq 0$. It follows that:

$$A_0 \equiv \lim_{\omega\to 0} A(\omega) = -\frac{R+1}{R}.$$

Thus, for $A < A_0$, the first bifurcation surface lies completely below the $A + B + C = 0$ plane. Provided all other bifurcation curves in the BC-plane at $A = A_0$ are simple, the D-decomposition partitions of El'sgol'ts [7] show that (3.2) has at least one root with Re $\lambda > 0$. This follows since below the $A + B + C = 0$ plane there is a unique positive root and above the $A + B + C = 0$ plane there are two complex roots with positive real part which must have crossed the imaginary axis with $0 < \omega < \frac{\pi}{(1-R)}$. The results of Appendix B are used to show that other bifurcation curves are simple when $R > R_0 \simeq 0.0117$.

When $A = A_0$, then (3.5) shows that $B_0 = R/(R-1)$ and $C_0 = 1/R(1-R)$. For $A > A_0$, one edge of the first bifurcation surface emanates along (3.5) in the $A+B+C = 0$ plane. As ω increases from zero, Eqn. (3.7) along with (3.4) is used to determine the other intersection of the first bifurcation surface with the $A + B + C = 0$ plane. Appendix A gives a proof that this portion of the first bifurcation surface lies above the $A + B + C = 0$ plane. As A continues to increase, there is some value of $A = A_1$ where another bifurcation surface (or possibly a section of the first bifurcation surface with higher values of ω, $R > \frac{1}{2}$) enters the boundary of the stability region. For $R_0 < R < \frac{1}{2}$ and $A = A_1$, often the second bifurcation self-intersects and begins a new region of stability that joins the principal region of stability described here at a larger value of A. For $A \in (A_0, A_1)$, the stability region is bounded by only the first bifurcation surface and the $A+B+C = 0$ plane. This completes the proof of the theorem.

For each fixed R, we begin our studies with $A = A_0$, then examine the evolution of the stability region as A increases. Theorem 3.2 shows that initially the stability region is enclosed by part of the first bifurcation surface and a section of the $A + B + C = 0$ plane. However, as A increases other bifurcation surfaces enter the boundary of the stability region in several ways. Below we define three methods by which bifurcation surfaces encroach upon the boundary of the stability region for $R \leq \frac{1}{2}$. In this paper we consider only the case $R \leq \frac{1}{2}$ since the bifurcation curves are simple for these delays, except possibly over a small range of A values. (See Appendix B for more details.) When $R > \frac{1}{2}$, the bifurcation surfaces typically self-intersect complicating the analysis. These delays are left for future research.

For most values of A, the curves in the BC-plane generated by (3.4) tend to infinity parallel to the lines $B+C = 0$ or $B-C = 0$, as $\omega \to \frac{j\pi}{1-R}$. However, for certain values of A, the equations given by (3.4) become indeterminate

at $\frac{j\pi}{1-R}$. Define these *transition* values of A by A_j^*, where

$$A_j^* = -\frac{j\pi}{1-R}\cot(\tfrac{jR\pi}{1-R}), \qquad j = 1, 2, ... \tag{3.8}$$

At a transition the j^{th} and $(j+1)^{\text{st}}$ bifurcation curves coincide at the specific point (B_j^*, C_j^*), where

$$\begin{aligned} B_j^* &= (-1)^j \frac{(1-R)\cos(\frac{jR\pi}{1-R}) - jR\pi\csc(\frac{jR\pi}{1-R})}{(1-R)^2}, \\ C_j^* &= -(-1)^j \frac{(1-R)\cos(\frac{j\pi}{1-R}) - j\pi\csc(\frac{j\pi}{1-R})}{(1-R)^2}. \end{aligned} \tag{3.9}$$

All along the line,

$$(B - B_j^*) + (-1)^j(C - C_j^*) = 0, \quad A = A_j^*, \tag{3.10}$$

there are two roots of (3.2) on the imaginary axis with $\lambda = \pm\frac{j\pi}{1-R}i$. If the j^{th} bifurcation surface is on the boundary of the stability region for A slightly less than A_j^*, then at $A = A_j^*$, Eqn. (3.10) becomes part of the stability region's boundary, and subsequently, the $(j+1)^{\text{st}}$ bifurcation surface enters the boundary of the stability region: Our studies show that the greatest local distortions in the stability surface occur near transitions. Appendix A provides analytical results for A_1^*.

From Appendix B, the $(j+1)^{\text{st}}$ bifurcation surface, which enters the boundary of the stability region immediately after A_j^*, self-intersects for a range of A values prior to the transition. The small region enclosed by the self-intersection contains no eigenvalues to (3.2) with positive real parts; hence, (3.1) is stable within this region. Following A backwards from A_j^*, we define A_j^p be the value where the area enclosed by the self-intersection goes to zero. For $A \in (A_j^p, A_j^*)$, there is a protrusion in the stability region or a *stable spur*, which joins the region of stability of Theorem 3.2 at A_j^*. In BC-cross sections the stable spur appears to be disconnected from the principal region of stability. The 3-dimensional structure maintains connectivity between the principal region of stability and the stable spur at the transitional value, A_j^*.

Theorem 3.1 demonstrates that for each A one corner of the MRS is given by $(B, C) = (0, -A)$. Eqn. (3.5) shows that the first bifurcation surface intersects the $A + B + C = 0$ plane at $(B, C) = ((AR+1)/(1-R), -(A+1)/(1-R))$, which diverges from $(0, -A)$ as A increases. Thus, a large gap develops between the first bifurcation surface and the lower corner of

the MRS where another bifurcation surface may join the boundary of the stability region. We define the *transferral* value of $A = A^z_{i,j}$ to be the value of A where the j^{th} bifurcation surface intersects the i^{th} bifurcation surface at the $A + B + C = 0$ plane with the j^{th} bifurcation surface entering the boundary of the stability region for $A > A^z_{i,j}$. This is a second way in which bifurcation surfaces enter the boundary of the stability region. Often there is only one transferral value, but for some values of R a distortion of the bifurcation surface near the $A + B + C = 0$ plane caused by a transition results in several transferrals.

The third route through which bifurcation surfaces enter the boundary of the stability region is a tangency. We define the *tangential* value of $A = A^t_{i,j}$, to be the value of A at which the j^{th} bifurcation curve becomes tangent to the i^{th} bifurcation curve, where the i^{th} curve is part of the stability boundary. As A increases from $A^t_{i,j}$, the new bifurcation curve is incorporated into the boundary of the stability region, separating segments of the bifurcation curve to which it was tangent.

For $R < \frac{1}{2}$ fixed, we determine the boundary of the stability region in the BC-plane by examining changes that occur as A increases. From the initial the point given in Theorem 3.2, additional bifurcation curves enter the boundary of the stability region by one of the methods listed above, *i.e.,* a transition (which includes an associated stable spur), a tranferral, or a tangency. The complete 3-dimensional bifurcation stability surface is generated by combining these cross-sectional graphs.

4 Example with Delay of $R = \frac{1}{3}$

In this section, we describe the stability region for the case $R = \frac{1}{3}$, using the definitions and theorems developed in the previous section. The 3-dimensional stability surface is presented in Fig. 4.1. Our choice of $R = \frac{1}{3}$ as the leading example stems from the organization of the bifurcation curves into four families with a single transition value $A^*_{2k+1} = 0$, for all $k = 0, 1, ...$ (There are no even transitions for $R = \frac{1}{3}$.) The relative simplicity of this case makes it easier to understand how the stability surface evolves. Many of the techniques illustrated here are applicable to other delays and with some modifications are demonstrated in subsequent sections.

The surface is created by fixing values of A and determining the stability region in the BC-cross-sectional plane. From Theorem 3.2, the stability

surface for $R = \frac{1}{3}$ comes to a point at

$$(A_0, B_0, C_0) = \left(-4, -\tfrac{1}{2}, \tfrac{9}{2}\right).$$

The first change in this stability surface occurs at the transitional value of A. From (3.8),

$$A_1^* = -\frac{3\pi}{2}\cot(\frac{\pi}{2}) = 0.$$

For $A \in (A_0, A_1^*) = (-4, 0)$, the stability region given by Theorem 3.2 is bounded by the first bifurcation surface (blue) and the $A+B+C = 0$ plane (violet).

As A approaches the transitional value $A_1^* = 0$, the region of stability expands as the first bifurcation curve is stretched along the line $C - B = \frac{3\pi}{2}$ toward the second bifurcation curve. Similarly, the second bifurcation curve is drawn toward the first bifurcation curve for A near A_1^*, causing the second bifurcation curve to self-intersect as seen in Fig. 4.2. This self-intersection only exists for $A \in (A_1^p, A_1^*) \simeq (-0.117, 0)$, and encloses another region of stability. This region of stability is too small to appear in Fig. 4.1, but the distortion is clear from the transition line in black that parallels the level curves in the top figure (just prior to the second bifurcation surface shown in green). The stable spur isolates this portion of the stability region as the second bifurcation curve self-intersects, creating a loop whose area increases as A approaches A_1^*. Though the BC-cross-section in Fig. 4.2 shows the two stable regions to be disjoint, connectivity is maintained in the 3-dimensional ABC-parameter space via the transition.

At the transition, $A_1^* = 0$, the first and second bifurcation curves meet at the point $(B_1^*, C_1^*) = (3\pi/4, 9\pi/4)$ as seen in Fig. 4.3. Along the line $C - B = \frac{3\pi}{2}$, which is derived from (3.10), the purely imaginary solutions $\lambda = \pm i\frac{3\pi}{2}$ satisfy (3.2). The region of stability from Theorem 3.2 is bounded by parts of the first bifurcation surface, the $A+B+C = 0$ plane, and the line $C - B = \frac{3\pi}{2}$. The stable spur is bounded by the second bifurcation surface and the line $C - B = \frac{3\pi}{2}$. The region of stability from Theorem 3.2 and the stable spur join at the point (B_1^*, C_1^*). Subsequently, the ends of the first and second bifurcation curves swap positions near $\omega = \frac{3\pi}{2}$. Fig. 4.4 shows how the first and second bifurcation curves comprise the boundary of the stability region for A slightly larger than A_1^*. For $A \in (A_1^*, A_{1,4}^z) \simeq (0, 7.1)$, the stability region is bounded by sections of the first bifurcation surface (blue), the second bifurcation surface (green), and the $A+B+C = 0$ plane. A magnified 3-dimensional picture of the transition, A_1^*, and its associated stable spur is shown in Fig. 4.5.

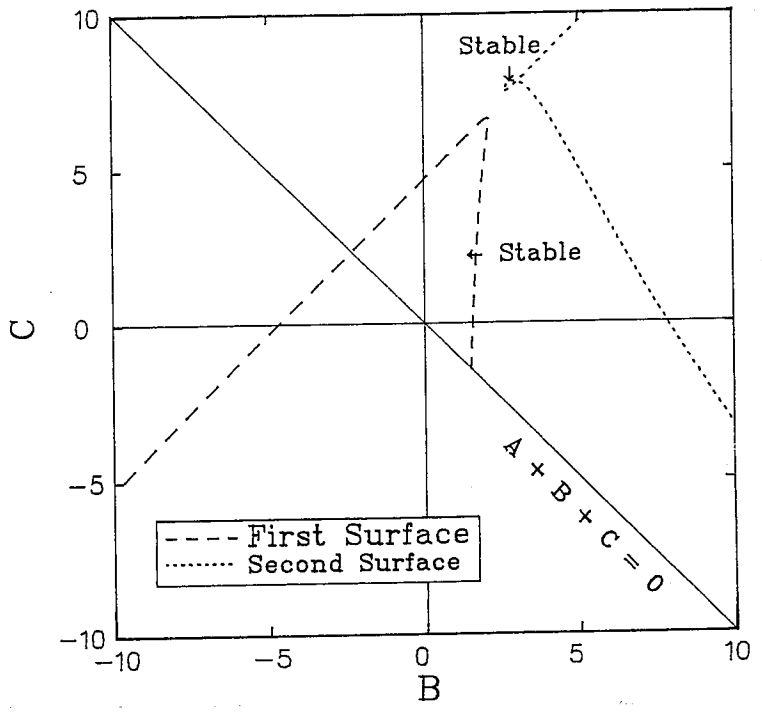

Figure 4.2: For $R = \frac{1}{3}$ and $A = -0.02$, the stability region is bounded by the first bifurcation curve and the line $A+B+C = 0$. A stable spur appears as the second bifurcation curve self-intersects.

At the transferral value $A = A^z_{1,4}$, the first bifurcation surface, the fourth bifurcation surface (red), and the $A+B+C = 0$ plane intersect at the point $(A, B, C) \simeq (7.1, 5.0, -12.1)$, where the fourth bifurcation surface enters the boundary of the stability region. For $A \in (A^z_{1,4}, A^t_{2,6})$, the stability region is bounded by sections of the first, second and fourth bifurcation surfaces and the $A + B + C = 0$ plane.

At $A = A^t_{2,6} \simeq 30.7$, the sixth bifurcation surface (orange) becomes tangent to the second bifurcation surface and subsequently joins the boundary of the stability region for $A > A^t_{2,6}$. This point of tangency is near $(A, B, C) = (30.7, -12.0, 33.8)$. The next change in the stability surface occurs at $A = A^t_{4,8} \simeq 50.4$, where the eighth bifurcation surface becomes tangent to the fourth bifurcation surface. This point of tangency is near $(A, B, C) = (50.4, 18.7, -54.1)$. As A increases further, additional tangencies occur, injecting more of the even bifurcation surfaces into the boundary of the stability region.

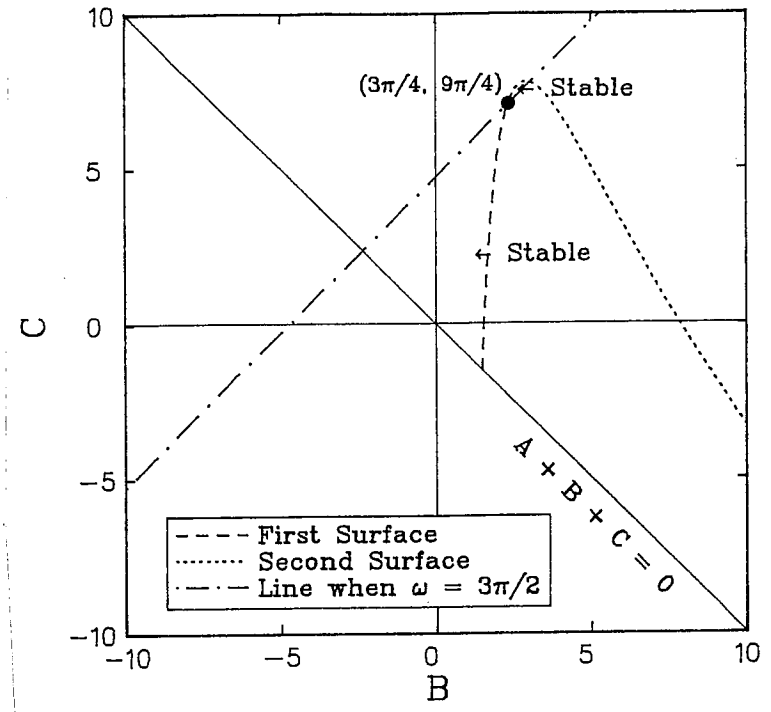

Figure 4.3: For $R = \frac{1}{3}$ and $A_1^* = 0$, a transition occurs. The stability region of Theorem 3.2 is bounded by the first bifurcation curve and the lines $B + C = 0$ and $C - B = \frac{3\pi}{2}$. The stable spur is bounded by the second bifurcation curve and the line $C - B = \frac{3\pi}{2}$ and joins the first region of stability at the point (B_1^*, C_1^*).

The results of the one delay problem in Section 2 show that the first bifurcation surface and the $A + B + C = 0$ plane always contribute to the boundary of the stability region near $C = 0$ for $A > A_0$. Our analysis using 2-dimensional cross-sections with increasing values of A establishes that the boundary of the stability region for $R = \frac{1}{3}$ only adds bifurcation curves from the second and fourth families. The curves of the first and third families do not affect the stability region except for the first bifurcation curve. See Appendix C for the derivation of these claims. This methodology allows us to completely characterize the region of stability in ABC-parameter space. In Section 7, we establish that the region of stability for $R = \frac{1}{3}$ remains bounded away from the MRS of Theorem 3.1. Our numerical studies show that the size of the stability region is proportional to A, provided A is sufficiently large, with the cross-sectional shape essentially unchanged as A

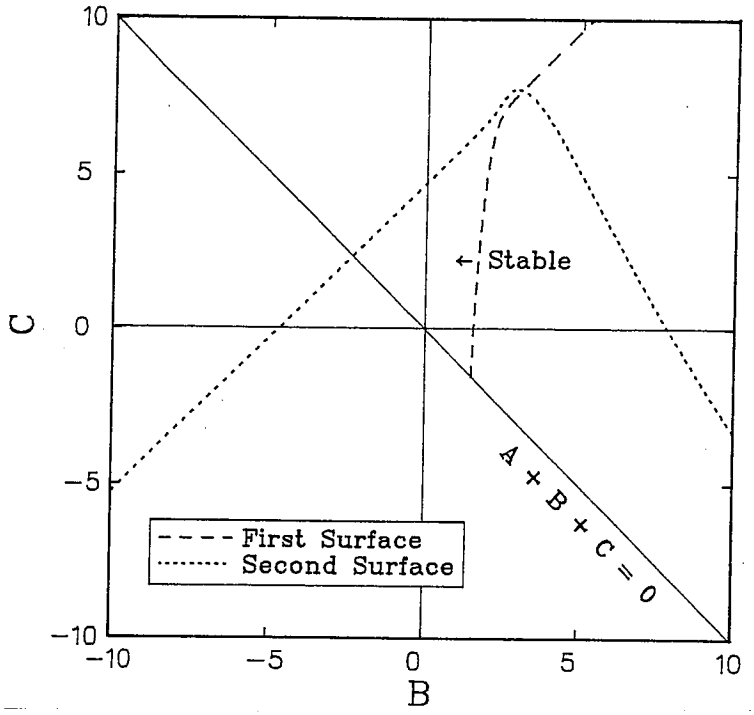

Figure 4.4: For $R = \frac{1}{3}$ and $A = 0.02$, the stability region is bounded by the first and second bifurcation curves and the line $A + B + C = 0$.

increases.

The transitional values of A are found by determining the value of A_j^* which make $B(\omega_j^*)$ and $C(\omega_j^*)$ indeterminate. This occurs when $\omega_j^* = \frac{3j\pi}{2}$, and Eqn. (3.4) shows that

$$A_j^* = -\frac{3j\pi}{2}\cot(\frac{j\pi}{2}).$$

It follows that $A_j^* = 0$ for j odd and $A_j^* = \infty$ for j even. Thus, all transitions occur at $A = 0$, affecting only the first and second bifurcation surfaces as depicted in Fig. 4.3. For delays other than $R = \frac{1}{3}$, transitions occur at various values, A_j^*, $j = 1, 2, ...$ and, as will be shown later, can significantly complicate the boundary of the stability region.

The behavior of the four families of bifurcation curves over a range of values of A and ω determine the geometry of the stability region. Fig. 4.6 shows a representative cross-section in the BC-plane, demonstrating the typical shapes of each family group. Familial characteristics are detailed below with the derivations contained in Appendix C.

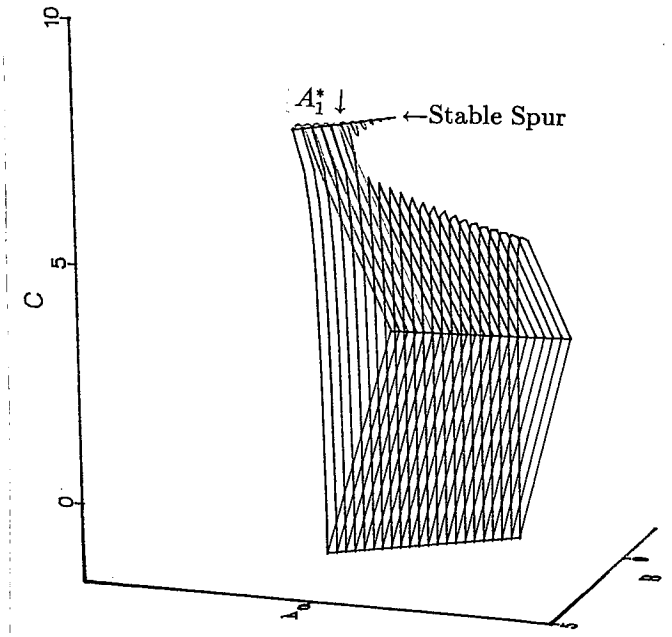

Figure 4.5: The stability surface for $R = \frac{1}{3}$ with $A \in [-0.3, 0.1]$. This figure magnifies the region which contains the transition, A_1^*, and its associated stable spur.

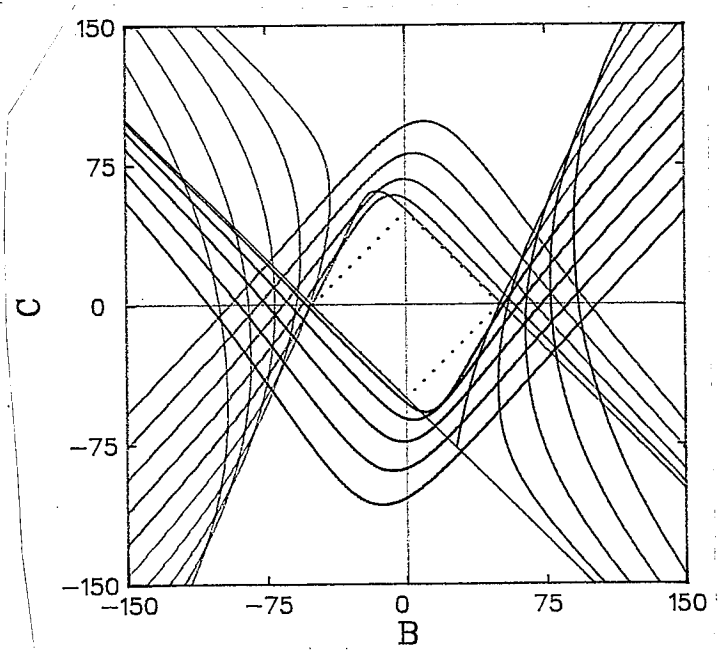

Figure 4.6: Cross-section in the BC-plane of the first 20 bifurcation curves for $R = \frac{1}{3}$ and $A = 50$. The four families of bifurcation curves are easily seen with the first, second, third, and fourth families represented by blue, green, orange, and red, respectively. The dotted line is the border of the Minimum Region of Stability.

From (3.5), the first bifurcation curve begins at the point $(B,C) = (\frac{A+3}{2}, -\frac{3(A+1)}{2})$, then as is shown in Appendix C, along this curve both B and C increase monotonically for $A > 0$. As noted above from the study of the one delay problem, this curve passes through the Hopf curve given in Fig. 2.1 for each value of A. This indicates that as A increases, the first bifurcation curve approaches the vertex of the MRS where $C = 0$ and $B = A$. As $\omega \to \frac{3\pi}{2}$, the first bifurcation curve becomes parallel to the line $B-C = A$. Other members of the first family of bifurcation curves are generated with values of $\omega \in (6k\pi, 6k\pi + \frac{3\pi}{2})$, where $k = 1, 2, ...$, and are depicted in blue in Fig. 4.6. Members of this family begin near the line $B + C = -A$. As ω increases, these curves eventually cross the first bifurcation curve at points increasingly farther away from its intersection with $C = 0$, reversing their initial order as seen in Fig. 4.6. As $\omega \to 6k\pi + \frac{3\pi}{2}$, members of the first family of curves become parallel to the line $B-C = A$ such that a constant distance of 6π is maintained between the tails of the first family of bifurcation curves. By examining Fig. 4.6 and given the structured ordering described above, one can readily see that this family does not influence the stability region except through its first member.

The third family is nearly a reflection of the first family, but does not possess any member that corresponds to the first bifurcation curve. The members of this family of curves are generated by (3.4) with $\omega \in (6k\pi + 3\pi, 6k\pi + \frac{9\pi}{2})$, where $k = 0, 1, 2, ...$, and are depicted in orange in Fig. 4.6. These curves begin near the line $B + C = A$ and have a crossing pattern similar to the first family's pattern, lying entirely outside the region of stability. The third family of curves mimicks the first family of curves, becoming parallel to the line $B - C = -A$ as $\omega \to 6k\pi + \frac{9\pi}{2}$.

The second and fourth families of bifurcation curves exhibit more interesting properties and are the most significant contributors to the boundary of the region of stability. From the one delay problem with $B = 0$ the first bifurcation curve passes through the scaled Hopf curve of Fig. 2.1 for $A < 0$. For $A > 0$, the second bifurcation curve creates the remainder of the stability boundary and approaches the vertex $(0, A)$ of the MRS in the BC-plane as $A \to +\infty$. The green arcs in Fig. 4.6 are the second family of bifurcation curves. As ω decreases to $6k\pi + \frac{3\pi}{2}$, these curves become parallel to the line $B-C = 0$ with the lower numbered members of the family closer to this line. As ω increases, each family member reaches a peak above the MRS, after which they asymptotically approach the line $B + C = A$ as $\omega \to 6k\pi + 3\pi$ for $k = 1, 2...$ Again the asymptotic order of the curves is maintained with

lower numbered members of the second family closer to the line $B+C=A$, as shown in Fig. 4.6.

The reason the second family's behavior is significant in determining the boundary of the stability region stems from the loss of curve ordering near the maximum of each curve. Fig. 4.6 shows the deformation of curves near the extremum that induces a sequence of intrafamilial tangencies as A increases. In this way several bifurcation curves of the second family enter the boundary of the region of stability. The first such intersection occurs when the second and sixth curves (the first and second members of the second family) become tangent near the point $(A,B,C)=(30.7,-12.0,33.8)$.

The fourth family of bifurcation curves ($\omega \in (6k\pi+\frac{9\pi}{2}, 6(k+1)\pi)$) is basically a reflection of the second family. While the second bifurcation curve provided the boundary along $B+C=A$, the fourth family lies below the $A+B+C=0$ line, and all members asymptotically approach this line for $\omega \to 6(k+1)\pi$. It is the fourth bifurcation surface that undergoes a transferral with the first bifurcation surface near $A^z_{1,4}=7.1$. The similarity of the fourth family curves to those in the second family is depicted in Fig. 4.6, including the intrafamilial intersections that lead to tangencies, the asymptotic limits, and order preservation as discussed above.

For any fixed value of A there is only a finite number of second and fourth family bifurcation curves that lie on the boundary of the stability region. After a finite number of curves have intrafamilial intersections, the remaining infinite number of curves in the second and fourth families are order preserving. Hence, these curves do not play any role in determining the boundary of the stability region. Since the number of curves on the boundary of stability region is finite for each cross-section in the BC-plane and because this number increases with A, we are able to completely characterize the stability region below any given value of A. This allows us the generate the 3-dimensional stability surface portrayed in Fig. 4.1.

5 Changes in the Stability Region for R near $\frac{1}{3}$

This section examines the local changes in the stability region that occur as R increases or decreases from $\frac{1}{3}$. For a certain range of A values and small variations in R, the structure of the stability region closely resembles the case $R=\frac{1}{3}$ studied in the previous section. However, there are important differences for values of R near $\frac{1}{3}$ as shown below. Our discussion in this

section focuses on changes in the stability region for $R \in [0.31, 0.35]$.

For R near $\frac{1}{3}$, the initial point on the boundary of the stability region, (A_0, B_0, C_0), is found using Theorem 3.2. The initial value A_0 increases smoothly with increasing R, while B_0 and C_0 both decrease. The theorem also shows that initially the stability surface consists only of parts of the first bifurcation surface and the $A + B + C = 0$ plane. It is easily seen that small changes in the delay result in only minor changes in the stability region when A is near A_0. Fig. 5.1 shows how little A_0 changes for $R \in [0.31, 0.35]$.

The first change in the stability surface of Theorem 3.2 for $R \in [0.31, 0.35]$ is the transition, A_1^*. Prior to A_1^*, the second bifurcation surface self-intersects creating a stable spur on the interval (A_1^p, A_1^*), which joins the stability surface of Theorem 3.2 at A_1^*. The length of the interval (A_1^p, A_1^*) decreases from 0.159 for $R = 0.31$ to 0.092 for $R = 0.35$, indicating that the stable spur is a minor part of the stability surface. Differentiating (3.8) shows that A_1^* increases monotonically with R, but the change in A_1^* is very small as shown in Fig. 5.1. Consequently, Figs. 4.2-4.5 are representative of the geometry of the stability surfaces near A_1^* for $R \in [0.31, 0.35]$. Immediately after the A_1^* transition, the stable spur disappears in BC-cross-sections, and the stability region is bounded by the first and second bifurcation surfaces and the $A + B + C = 0$ plane.

As A increases, Fig. 5.1 shows that for most values of $R \in [0.31, 0.35]$ the next change in the stability surface is the tranferral, $A_{1,4}^z$, as is the case when $R = \frac{1}{3}$. However, near $R \simeq 0.311$ this transferral no longer occurs due to another transition, A_4^*. As R decreases from $\frac{1}{3}$, the value A_4^* decreases with the transition occurring along the line given by (3.10), which can be shown to lie below the $A + B + C = 0$ plane. This decrease in A_4^* causes the fourth bifurcation surface to extend out further for its transferral value as it smoothly approaches (3.10). Near $R \simeq 0.311$, A_4^* has sufficiently stretched the fourth bifurcation surface so that the first transferral does not occur until after A_4^*. For a range of $R < 0.311$, the fifth bifurcation surface becomes the first transferral, $A_{1,5}^z$. Prior to this transferral, there is another change in the stability surface when $R < 0.311$ due to the second transition, A_2^*.

For $R \in (0.311, 0.325)$, the stability surface changes in a manner quite different from the case $R = \frac{1}{3}$. Rather than the next change in the stability surface being the tangency, $A_{2,6}^t$, as A increases, a reverse transferral, $A_{4,1}^z$, appears where the first bifurcation surface displaces the fourth bifurcation surface. (See Fig. 5.2.) In the case $R = 0.32$, the fourth bifurcation surface is incorporated into the stability region boundary at $A_{1,4}^z \simeq 8.86$, then

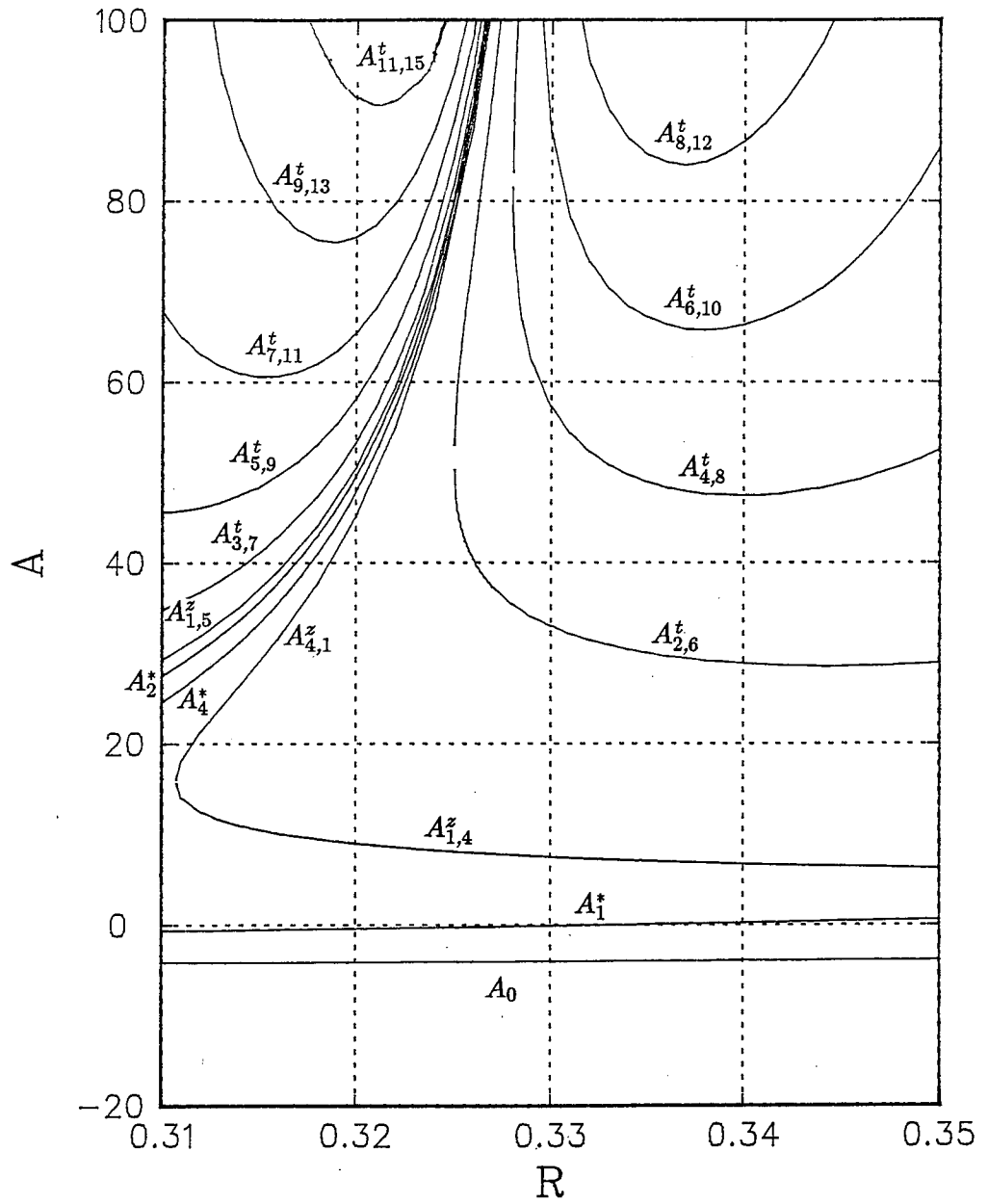

Figure 5.1: This figure shows the values of A_0 and various transitions, transferrals, and tangencies for $R \in [0.31, 0.35]$, which affect the geometry of the stability region for $A \leq 100$. Note that some transitions are omitted for clarity.

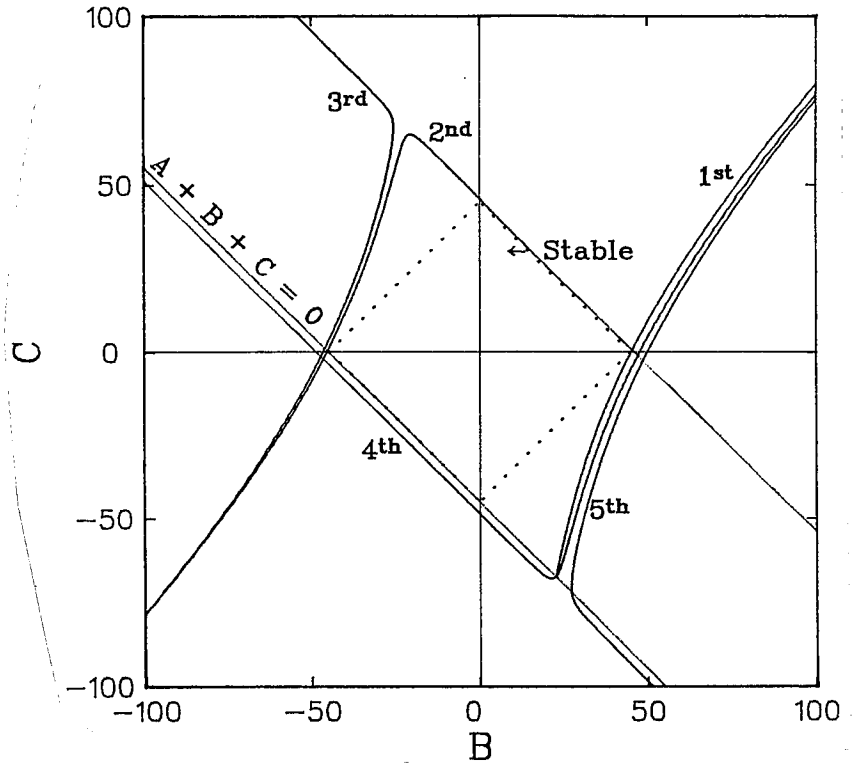

Figure 5.2: When $R = 0.32$, a reverse transferral occurs at $A^z_{4,1} \simeq 45.0$. This figure shows the first five bifurcation surfaces.

leaves the boundary at $A^z_{4,1} \simeq 45.0$. The geometry of this reverse transferral departs from the example of $R = \frac{1}{3}$ presented in Section 4 where all curves that join the boundary of the stability region remain part of it.

As A increases further, the second transition, A^*_2, causes the next change in the stability surface and results in the third bifurcation surface becoming part of the boundary. The resulting distortion in the shape of the stability surface is depicted in Fig. 5.3. The transitions A^*_2 and A^*_4 are very close in value for the given range of R. For example, when $R = 0.32$, $A^*_2 \simeq 49.4$ and $A^*_4 \simeq 47.7$. These transitions cause the stability region to extend along the $B + C = \pm A$ lines that bound the MRS and significantly increase the size of the region of stability for a range of A values. All stability surfaces with $R \in [0.31, \frac{1}{3})$ are affected by A^*_2 and have similar distortions. In addition, these transitions have associated stable spurs on the interval (A^p_2, A^*_2) as the

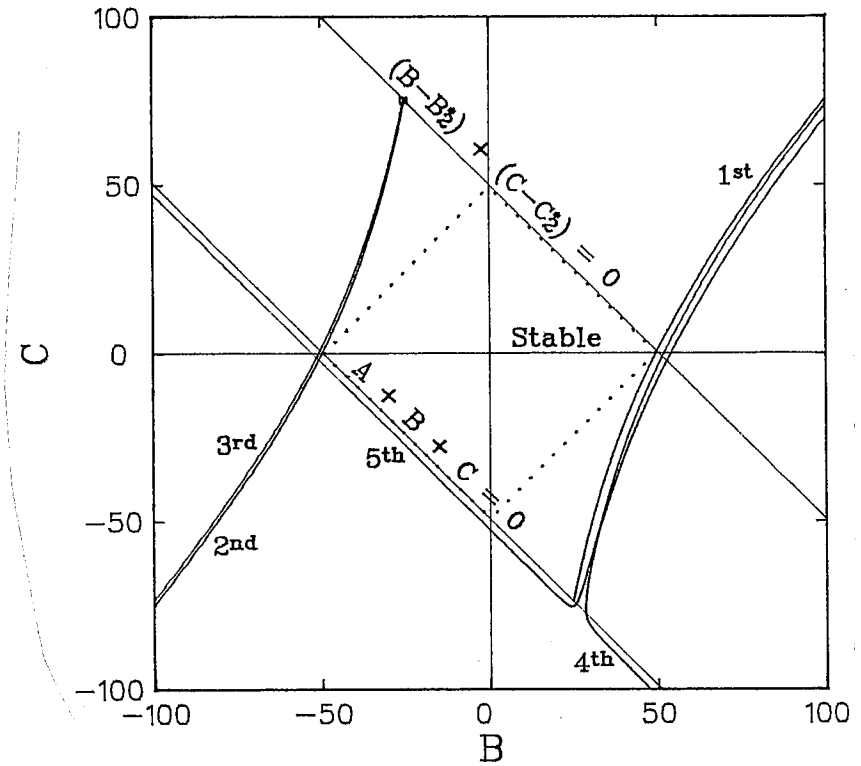

Figure 5.3: When $R = 0.32$, a transition occurs at $A_2^* \simeq 49.43$. This figure shows the first five bifurcation surfaces and the line at the transition, $(B - B_2^*) + (C - C_2^*) = 0$.

third bifurcation curve self-intersects. These stable spurs are much smaller than the ones associated with A_1^*. For example, $A_2^* - A_2^p \simeq 4.88 \times 10^{-4}$ at $R = 0.31$ and decreases to $A_2^* - A_2^p \simeq 2.63 \times 10^{-4}$ when $R = 0.32$.

Fig. 5.4 graphs the next change in the boundary of the stability region as the transferral $A_{1,5}^z$ occurs. For $R \in [0.31, 0.311)$ the sequence of changes in the stability region are simpler as the fourth bifurcation surface never enters the boundary of the stability region via a transferral, as seen in Fig. 5.1.

For $R \in [0.325, 0.35]$, the next change in the boundary of the stability region after $A_{1,4}^z$ is the tangency $A_{2,6}^t$. On this interval the next change depends on which subinterval is considered. For $0.329 < R \leq 0.35$ and $A \leq 100$, Fig. 5.1 shows that the stability surface undergoes a series of tangencies similar to the ones discussed for $R = \frac{1}{3}$. However, for lower

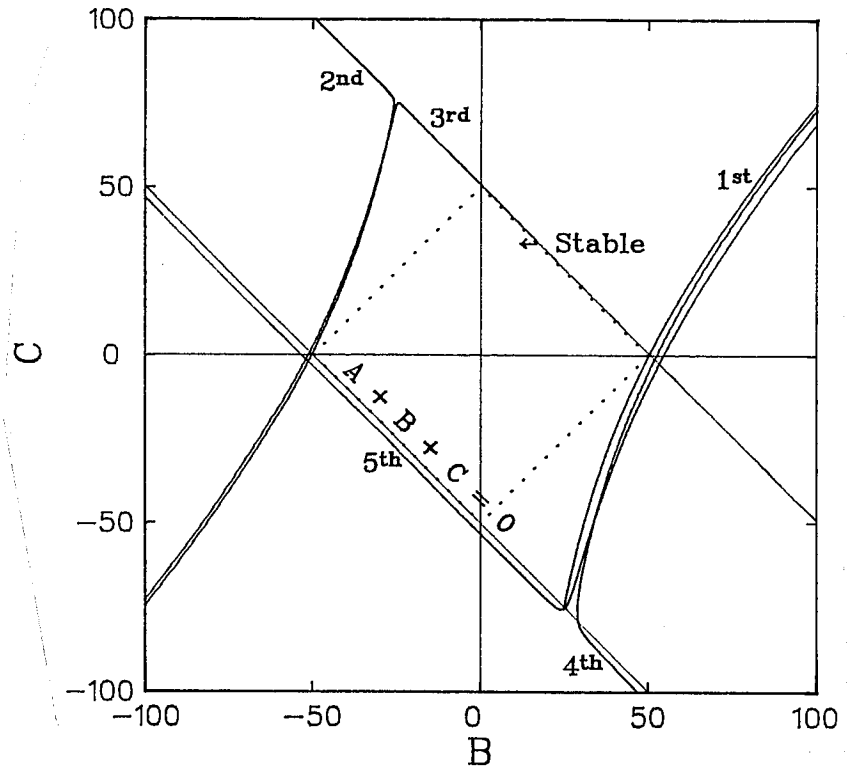

Figure 5.4: When $R = 0.32$, another transferral occurs at $A^z_{1,5} \simeq 50.4$. This figure shows the first five bifurcation surfaces.

values of R, once again several transitions affect the geometry of the stability surface. For example, consider $R = 0.326$, where $A^t_{2,6} \simeq 40.4$, $A^*_2 \simeq 90.6$, and $A^*_6 \simeq 88.0$. (Note that A^*_6 is not shown in Fig. 5.1; however, it lies close to and below A^*_4.) As A increases toward A^*_2 and A^*_6, the second and sixth bifurcation surfaces extend along the line $B + C = A$, and the tangency surface disappears at $A^t_{6,2} \simeq 74.4$. After the reverse transferral at $A^z_{4,1} \simeq 88.2$, the transition at $A^*_2 \simeq 90.6$, and the appearance of the new transferral surface at $A^z_{1,5} \simeq 91.1$, the tangency that disappeared reappears at $A^t_{3,7} \simeq 92.6$ with the third and seventh bifurcation surfaces taking the place of the second and sixth bifurcation surfaces. Each of these events causes different bifurcation surfaces to join the boundary of the stability region, hence different eigenvalues cause the Hopf bifurcation.

The discussion above shows that for $R < \frac{1}{3}$ even small changes in the de-

lay R may induce a significantly different set of bifurcation surfaces to bound the stability region. Most of these changes result from an even transition or series of even transitions, A^*_{2j}, that cause distortions along the $B+C=\pm A$ lines and do not occur when $R=\frac{1}{3}$. As seen in Fig. 5.1, the evolution of the stability surface for $R\in[\frac{1}{3},0.35]$ and $A\leq 100$ is much less dramatic.

So how do the odd transitions affect the boundary of the stability region? To examine this issue we consider $R=0.35$ and $A<250$. Fig. 5.5 shows how A^*_{11}, $A^t_{8,12}$, and $A^t_{8,11}$ vary with R. For $R=0.35$, a tangency occurs at $A_{8,11}\simeq 144$. As A increases, a transition occurs at $A^*_{11}\simeq 216$, which causes the 11^{th} bifurcation surface to be replaced by the 12^{th} bifurcation surface. This is a smooth transition parallel to the line $B-C=A$ and results in little noticeable change in the geometry of the stability region. Thus, odd transitions near $R=\frac{1}{3}$ affect which bifurcation surface is on the boundary of the stability region according to our definitions, but have little influence on the geometry of the region or the value of the eigenvalues involved in the Hopf bifurcation. The only effect of the A^*_{11} transition is to swap the 11^{th} and 12^{th} bifurcation surfaces in the boundary of the stability region.

The key to developing the 3-dimensional stability region is determining the junctures where changes in the stability surface occur. When two bifurcation surfaces meet on the stability surface, they share the same (A,B,C) value, and two pairs of purely imaginary eigenvalues, $\lambda=i\omega$, each satisfying (3.4) for a given A. Numerically, the two pairs of eigenvalues are found by Newton's method and are followed in 3-dimensions by slowly increasing A. Once the ω values are found for the ends of a bifurcation curve in the BC-cross-sections, then (3.4) is used to generate this segment along the boundary of the stability region. Thus, the most difficult part of the problem is determining which bifurcation surfaces comprise the boundary of the stability region and the values of A at which they enter. Fig. 5.1 provides an overview of changes in the stability region boundary as a function of A, listing the type of change in each case. Figs. 5.6-5.10 show the 3-dimensional structure of the stability regions for $R=0.31,0.32,\frac{1}{3},0.34,0.35$, respectively, and $A\leq 100$. These graphs are plotted using several colors to emphasize the similarities and differences in their stability regions.

As a supplement to the discussion above, a comparision is made among the 3-dimensional graphs presented in Figs. 5.6-5.10, indicating the significance of the color coded surfaces. For reference, the $A+B+C=0$ plane, where a real root crosses the stability surface, is always shown in violet. All of the graphs begin at the point (A_0,B_0,C_0), which we noted varies very

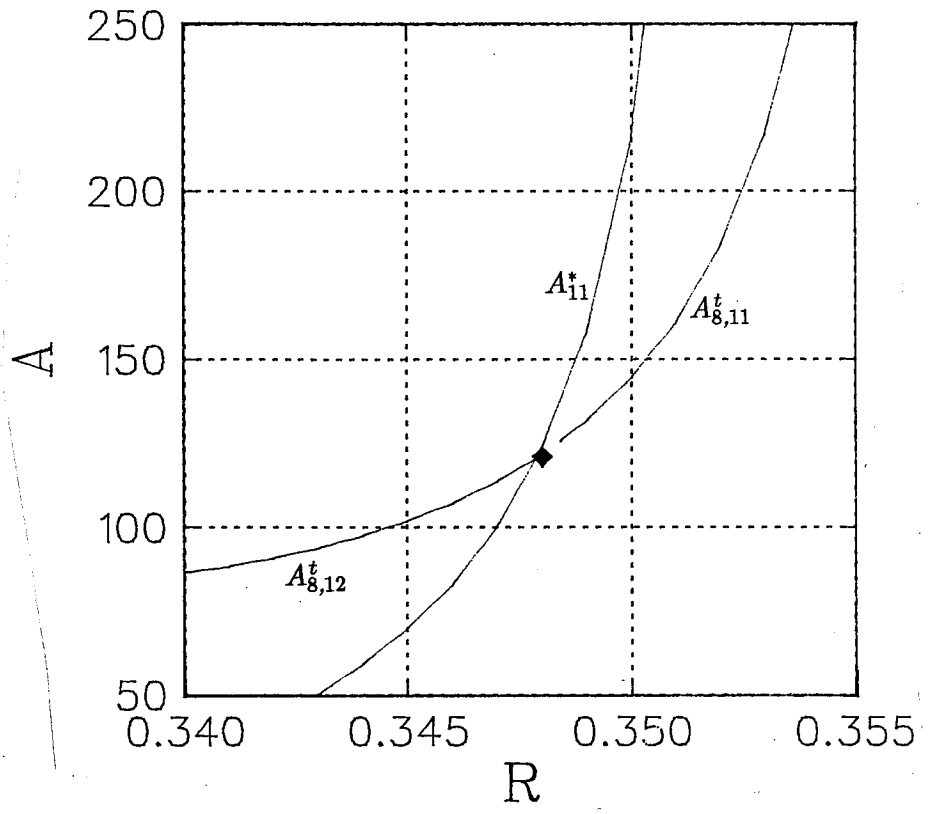

Figure 5.5: This figure shows the interaction between the transition A^*_{11} and the tangencies $A^t_{8,12}$ and $A^t_{8,11}$ for $R \in [0.34, 0.355]$.

little for $R \in [0.31, 0.35]$, and is clearly visible in each of the side perspectives. From this initial point the blue first bifurcation surface rises above the $A + B + C = 0$ plane, then is soon joined by the green second bifurction surface via the transition A^*_1. The graphs are drawn with a small small black line segment at A^*_1, but distortions due to transitions are diminished given the scale of the drawings. Also, because of the scale of the graphs, stable spurs are too small to be visible.

Graphically, the five stability surfaces resemble one another in the early stages in their evolution due to the continuity between delays. However, the 3-dimensional graphs clearly show dissimilarities between the cases $R < \frac{1}{3}$ and $R \geq \frac{1}{3}$, though some geometric resemblence is maintained. For the sequence of graphs in Figs. 5.8-5.10, the next change in the stability surface following the A^*_1 transition is the transferral, $A^z_{1,4}$. This transferral appears

in the figures as the red 4^{th} bifurcation surface enters the stability surface above the $A+B+C=0$ plane and encroaches upon the blue first bifurcation surface. After $A^z_{1,4}$, the only changes seen in the stability region for $A \leq 100$ are surfaces appearing through tangencies, which are caused by higher frequency Hopf bifurcations. Looking at the top graphs in Figs. 5.8-5.10, we see that the sequence of tangencies, $A^t_{2,6}$, $A^t_{4,8}$, $A^t_{6,10}$, and $A^t_{8,12}$ (the latter not appearing for $R=0.35$), alternates with first the orange 6^{th} bifurcation surface appearing in the upper left portion of the stability surface, then the blue 8^{th} bifurcation surface in the lower right portion, then the green 10^{th} bifurcation surface again above and to the left, and finally the red 12^{th} bifurcation surface in the lower right portion of the stability surface.

The sequence of changes as seen by our color coding is the same for Figs. 5.8-5.10, although for $R=0.35$ it can be seen that by $A=100$ the stability boundary is nearly a square, indicating its approach to the MRS. In fact, the cross-sectional area at $A=100$ is only 7.96% larger than the MRS for $R=0.35$, while it is 27.1% larger for $R=\frac{1}{3}$.

For $R<\frac{1}{3}$, the most prominent change in the 3-dimensional stability surface is A^*_2, which occurs near $A=30$ for $R=0.31$ and $A=50$ for $R=0.32$. In the top graphs for Figs. 5.6 and 5.7, the transition A^*_2 is recognizable in the replacement of the green 2^{nd} bifurcation surface with the red 3^{rd} bifurcation surface in the upper right portion of the stability surface. As A increases, the 3^{rd} bifurcation surface expands and displaces more of the 2^{nd} bifurcation surface. For $R=0.31$ and $R=0.32$, all of the even transitions occur near A^*_2, which induces a different set of bifurcation surfaces to enter the stability region boundary through transferrals and tangencies as indicated by the variation in the color coding.

A unique feature for $R=0.32$ among the depicted graphs is the appearance of the red 4^{th} bifurcation surface due to a transferral at $A^z_{1,4} \simeq 8.86$ that terminates in a reverse transferral near $A^z_{4,1}=45.0$. In both Figs. 5.6 and 5.7, the transition, A^*_4, introduces a new transferral, $A^z_{1,5}$, with the orange 5^{th} bifurcation surface displacing the first bifurcation surface. As noted earlier in this section, the transitions, A^*_2 and A^*_4, cause the stability surface to extend out along the planes $B+C=\pm A$. In the side view of Figs. 5.6 and 5.7 these transitions result in noticeable bulges in the stability surfaces. After the transferral, $A^z_{1,5}$, the remainder of the changes in the stability surfaces for $R=0.31$ and 0.32 and $A \leq 100$ are sequences of tangencies, $A^t_{3,7}$, $A^t_{5,9}$, $A^t_{7,11}$, $A^t_{9,13}$, and $A^t_{11,15}$ (the last two only appear in Fig. 5.7). Again the tangencies appear in an alternating pattern between the upper left and

lower right portions of the stability surface in the top figures with different colors indicating which odd numbered bifurcation surfaces are involved.

Ignoring the color coding which signifies the particular bifurcation surfaces on the boundary of the stability region at $A = 100$, we observe that Fig. 5.6 has more similarities in the shape of its stability region with Fig. 5.10 than any of the other stability surfaces. At $R = 0.31$ and $A = 100$, the stability surface is only 11.1% larger that the MRS. Thus, as R increases or decreases from $R = \frac{1}{3}$ (at least locally), the stability region appears to approach the MRS asymptotically in A. This phenomenon is described in Section 7 in more detail.

This section has demonstrated a methodology used to construct the boundary of the stability region as R changes over a limited range of values by applying the concepts developed in Section 3. In the next section we extend this process for a larger range of R values. Most significantly, we have shown that for a bounded region of R and A, there are only a finite number of bifurcation surfaces that need to be considered in the construction of the stability region boundary and that local continuity with respect to the parameters allows us to track the evolution of the boundary.

6 Extensions of the Geometric Analysis for $R \leq \frac{1}{2}$

In Section 4, the stability surface for (3.1) with $R = \frac{1}{3}$ was analyzed, and in the subsequent section the evolution of the stability surface for a range of R values near $R = \frac{1}{3}$ and A bounded was developed. Herein we extend the analysis of the previous section to delays in the range $0 < R \leq \frac{1}{2}$ for a bounded domain of A. We identify some generic properties of stability surfaces and discuss variations in the construction of the stability region boundary. Extensive numerical studies have established that new bifurcation surfaces enter the boundary of the stability region only through transitions (with associated stable spurs), tangencies, or transferrals as defined in Section 3. Fig. 6.1 shows the first transition, tangency, and transferral that affect the boundary of the stability region for $R \leq \frac{1}{2}$ and $A \leq 100$.

In Section 5, the transition A_1^* for $R \in [0.31, 0.35]$ was shown to be the first change affecting the boundary of the stability region given by Theorem 3.2, which consists of the first bifurcation surface and the $A+B+C = 0$ plane. In fact, we can show numerically that A_1^* is the first change in the stability boundary for all $R_0 < R < 0.47$. Recall that the transition A_1^*

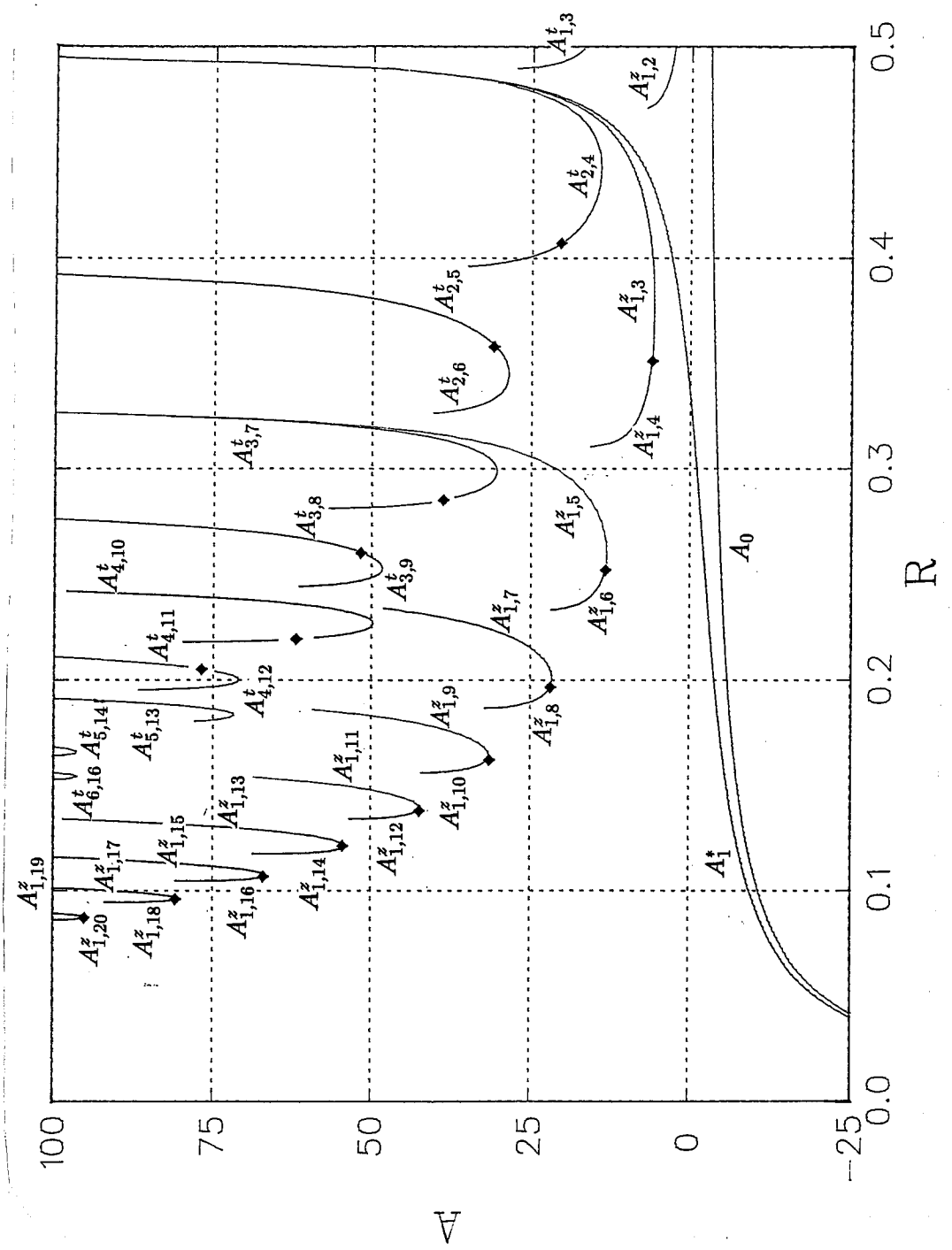

Figure 6.1: This figure shows the values of A_0, A_1^*, and various transferrals and tangencies for $R \in (0, \frac{1}{2}]$, which affect the geometry of the stability region for $A \leq 100$.

has an associated stable spur extending over the range $A \in (A_1^p, A_1^*)$ due to the self-intersection of the second bifurcation surface. Thus, as A increases from A_0 the stability region gains an additional area of stability at $A = A_1^p$, with BC cross-sections showing disjoint stability regions. Numerical studies show that the length of these stable spurs decreases as R increases.

Fig. 6.1 shows that A_1^* increases monotonically in R, with asymptotes at $R = 0$ and $R = \frac{1}{2}$. This figure does not include other transitions which may affect the boundary of the stability region. Nevertheless, the influence of these transistions can be surmized from the figure. Even numbered transistions cause the asymptotes in the transferral and tangency curves, partitioning the figure into a set of continuous curves. Each transferral pair, $A_{1,2n}^*$, $A_{1,2n+1}^*$, is circumscribed by even transistion asymptotes and is bisected by an odd transistion at the point indicated by a diamond. Lying above every adjacent transferral pair are two tangency curves, also bisected by odd transistions at the diamond. As R decreases from $\frac{1}{2}$, the transferral and tangency curves narrow with the minimum of each curve increasing as $R \to 0$. Moreover, higher frequency transitions decrease the gaps between transferral and tangency curves, as can be seen from the period of the cotangent function in (3.8). When R is small, tangencies and tranferrals do not occur until A becomes large. As a result, when R is near zero a large number of transitions contribute to the boundary of the stability region.

In order to illustrate effects that transitions have on the boundary of the stability region as R varies, we examine several examples from $R \in (0, \frac{1}{2}]$. At $R = \frac{1}{2}$, there are no transitions, and the stability region is comprised of only two families of bifurcation curves. A transferral occurs at $A_{1,2}^z \simeq 2.61$, after which all other changes to the stability region are the result of tangencies with the first occurring at $A_{1,3}^t \simeq 16.6$.

In Section 5 we saw that for the delays $R = \frac{1}{3}, 0.34, 0.35$, A_1^* is the only transition that influences the boundary of the stability region for $A \leq 100$, while both A_1^* and A_2^* influence the boundary of the stability region for $R = 0.31$ and 0.32. Appendix B demonstrates that these transitions have associated stable spurs. The length of the interval (A_1^p, A_1^*), where the stable spurs occur, ranges from 0.092 for $R = 0.35$ to 0.159 for $R = 0.31$. For $R \in [0.31, 0.35]$, stable spurs appear over a limited interval of A values, and their enclosed volume is relatively small compared to the the stability region beginning at A_0 as seen in Fig. 4.5. An additional effect induced by transitions can be seen in the case $R = 0.32$, where A_4^* causes a change in the transferral ordering through a distortion of the stability region along the

$A + B + C = 0$ plane.

Further from $R = \frac{1}{3}$, a distinctly different sequence of events occurs in the construction of the boundary of the stability region. In the case $R = 0.1$ with $A \leq 100$, there are no tangencies though a transferral occurs at $A^z_{1,17} = 91.7$. On the other hand, there are eight transitions, $A^*_i = -9.59, -8.32, -6.05, -2.46, 3.08, 12.09, 29.12, 76.72$, $i = 1, \ldots, 8$, which affect the boundary of the stability region. Each transition causes a new bifurcation surface to enter the boundary of the stability region, increasing its geometric complexity. The stable spurs associated with the transitions, $A^*_i, i = 1, \ldots, 8$, have interval lengths (A^p_i, A^*_i) of 0.688, 0.449, 0.277, 0.156, 0.076, 0.029, 0.007, and 0.001, respectively. Thus, stable spurs are smaller for higher frequency transitions. Unlike previous cases discussed, the stable spur originating from A^*_1 when $R = 0.1$ is relatively large compared to the stability surface emanating from A_0. The length of the interval (A^p_1, A^*_1) is 49% of the length of the interval (A_0, A^*_1), so locally this stable spur represents a significant portion of the stability region. This is shown in Fig. 6.2 for a cross-section at $A = -9.6$. Nevertheless, given the scale of Fig. 6.2, the area of the stable spur relative to the entire stability region is still quite small. An estimate of the total area of stability is approximately $\frac{1}{4}$ square unit.

Transitions, especially the even ones, have the greatest effect on the geometry of the stability region and the eigenvalues that determine stability, although transferrals and tangencies also contribute to the composition of the stability region. For example, when $0.47 < R < \frac{1}{2}$, the first change in the stability region is a transferral, as seen in Fig. 6.1. As R decreases, the figure shows that the first transferral occurs for increasingly higher bifurcation surfaces due to intervening transitions. For most values of $R \in (0, \frac{1}{2}]$, there is only one transferral that impinges on the boundary of the stability region. This figure does not illustrate the reverse transferrals which occur as a result of even transitions distorting a bifurcation surface along the $A + B + C = 0$ plane, but these would appear in the figure at the jump between $A^z_{1,2n}$ and $A^z_{1,2n+1}$ due to A^*_{2n} as R decreases. In Section 5, this situation was described in detail for $R = 0.32$ with Figs. 5.2-5.4 depicting changes in the geometry of the stability region.

The markers on the transferral curves in Fig. 6.1 indicate odd transitions which determine the particular bifurcation surface involved in a transferral. The figure shows that the change in A with respect to R is continuous for odd transitions along these transferrals. As a result, the geometric appearence of the stability region is maintained as A passes through an odd transition.

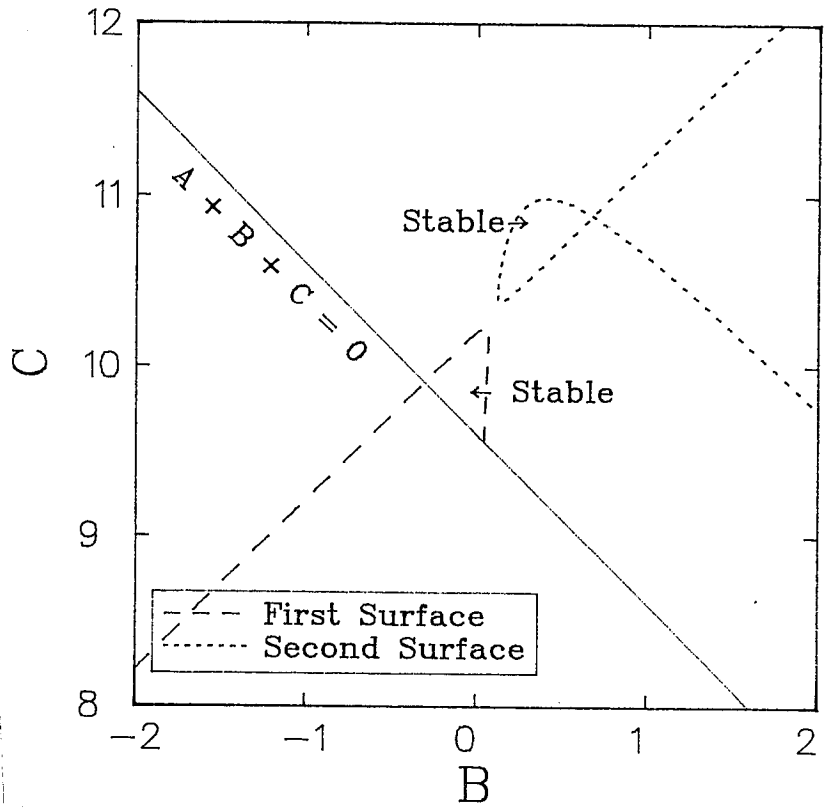

Figure 6.2: A magnified BC cross-section at $A = -9.6$ when $R = 0.1$ showing that the area of the stable spur can approach the size of the stability region emanating from A_0.

For example, when $R = 0.351$, A_3^* causes the fourth bifurcation surface to replace the first bifurcation surface as one of the surfaces intersecting the $A + B + C = 0$ plane, while at $R = 0.352$, it is the third bifurcation surface which enters the boundary of the stability region. However, $A_{1,4}^z \simeq 6.09$ at $R = 0.351$, and $A_{1,3}^z \simeq 6.00$ at $R = 0.352$, showing little change in the A value.

A pattern can also be discerned from Fig. 6.1 for tangencies. The figure shows two curves lying above each transferral curve which mimic its shape. Thus, the first tangency always occurs after the first transferral. As noted in Section 5, there are cases near even transitions where a surface enters and leaves via a tangency and then reappears on a higher frequency bifurcation surface, often with distortions in the shape of the stability region.

Like transferrals, odd transitions result in a change in the number of the bifurcation surfaces involved in a tangency, but the change in A, where the tangency occurs, is continuous in R. Unlike transferrals, after the appearance of the first tangency, many more follow. As R approaches $\frac{1}{2}$, tangencies play an increasingly important role in shaping the boundary of the stability region for a given bounded A.

The analysis of this section has shown that there is not a predictable pattern in the evolution of the stability surface for $R \in (0, \frac{1}{2})$. However, we have discovered some guiding principles using numerical schemes for determining the region of stability for any delay $R_0 < R \leq \frac{1}{2}$. The initial point A_0 as given by Theorem 3.2 is always the genesis of the stability region. The location of critical A values where transitions occur can be found from (3.8). When transitions involve one of the surfaces on the boundary of the stability region, changes in the geometry of the region occur. Prior to a transition, surface self-intersection adds stable spurs to the stability region. The relative size of the stability region due to a stable spur increases as $R \to 0$. Figs. 5.1 and 6.1 can be used to locate transferrals and tangencies and determine which curves are on the boundary of the stability region for a given R. In addition, these figures indicate the sensitivity of the stability region to perturbations in R for bounded values of A. A characterization of the stability region when A is unbounded is the topic of the next section.

7 Asymptotics

In Section 5, the 3-dimensional stability surfaces of Figs. 5.6-5.10 showed that the region of stability is larger than the MRS given in Theorem 3.1 for $A \leq 100$. In this section we examine the behavior of the stability region for $R \in (0, \frac{1}{2}]$ when A is large. Numerical studies indicate that for most delays the region of stability appears to asymptotically approach the MRS, although certain rational delays result in larger stability regions. Specifically, we show which rational values of R produce the largest regions of stability as $A \to +\infty$.

Fig. 2.1 reveals how the first bifurcation curve of the one delay problem approaches the $A = B$, $C = 0$ edge of the MRS as A becomes large. Similarly, a rescaling shows a set of bifurcation curves approaching the $A = C$, $B = 0$ edge of the MRS. The set of bifurcation surfaces along this edge as A increases is a progression from the first bifurcation surface to the m^{th}

bifurcation surface, where m is the least integer greater than or equal to $\frac{1-R}{R}$. Though the stability region approaches the MRS, the asymptotic behavior of the entire stability surface is highly dependent on R and may not approach all faces of the MRS.

To illustrate differences in the asymptotic behavior of the stability region for (3.1), we consider the delays $R = 0.5$ and 0.49. In a cross-section at $A = 100$, Fig. 7.1 shows the boundaries of the stability regions for $R = 0.5$ and 0.49, which are constructed from the first 10 and 16 bifurcation curves, respectively. At $A = 100$, the stability regions for $R = 0.5$ and 0.49 appear similar in the general shape and positioning of the bifurcation curves as might be expected from the continuous dependence of (3.2) on R. Furthermore, the respective stability regions for $R = 0.5$ and 0.49 are approximately 67.9% and 60.7% larger than the MRS at $A = 100$. However, unlike the delay $R = 0.5$, the transition A_1^* and several other transitions appear when $A < 100$ for $R = 0.49$. These transitions cause the upper portion of the stability region to be formed by the even bifurcation curves for $R = 0.49$, while the upper portion of the stability region for $R = 0.5$ uses only odd bifurcation curves. Though the shapes of the bifurcation curves are similar, their orientation is reversed in these two examples, indicating that the respective Hopf bifurcations occur at different locations on the imaginary axis. Thus, despite the geometric similarities of the stability regions in Fig. 7.1, the frequencies at which stability is lost are dissimilar, revealing a divergence in the construction of stability surfaces for these delays.

Eqn. (3.4) shows that as ω increases the bifurcation curves generated from two distinct delays will diverge even when the difference between the delays is small. As a result, the location in the BC-plane of the n^{th} bifurcation curves for two nearby R values may be quite different. Consider Fig. 7.2 in which the stability regions for $R = 0.5$ and 0.49 at $A = 400$ are composed of the first 38 and 26 bifurcation curves, respectively. Since a large number of bifurcation surfaces are required to construct the boundary of the stability regions for these examples, it is not surprising that geometric disparities emerge. Numerical integration at $A = 400$ indicates that relative to the MRS the area of the stability region for $R = 0.5$ is still approximately 67.8% larger, while the area of the stability region for $R = 0.49$ is only 7.5% larger. Thus, the shape of stability region at $R = 0.5$ persists as A increases with two nearly symmetric areas extending well beyond the MRS along the faces $B+C = A$ and $B-C = A$. On the other hand, the stability region for $R = 0.49$ is nearly coincident with the MRS at $A = 400$. The variation between between Figs. 7.1 and 7.2 demonstrates the sensitivity of the stability

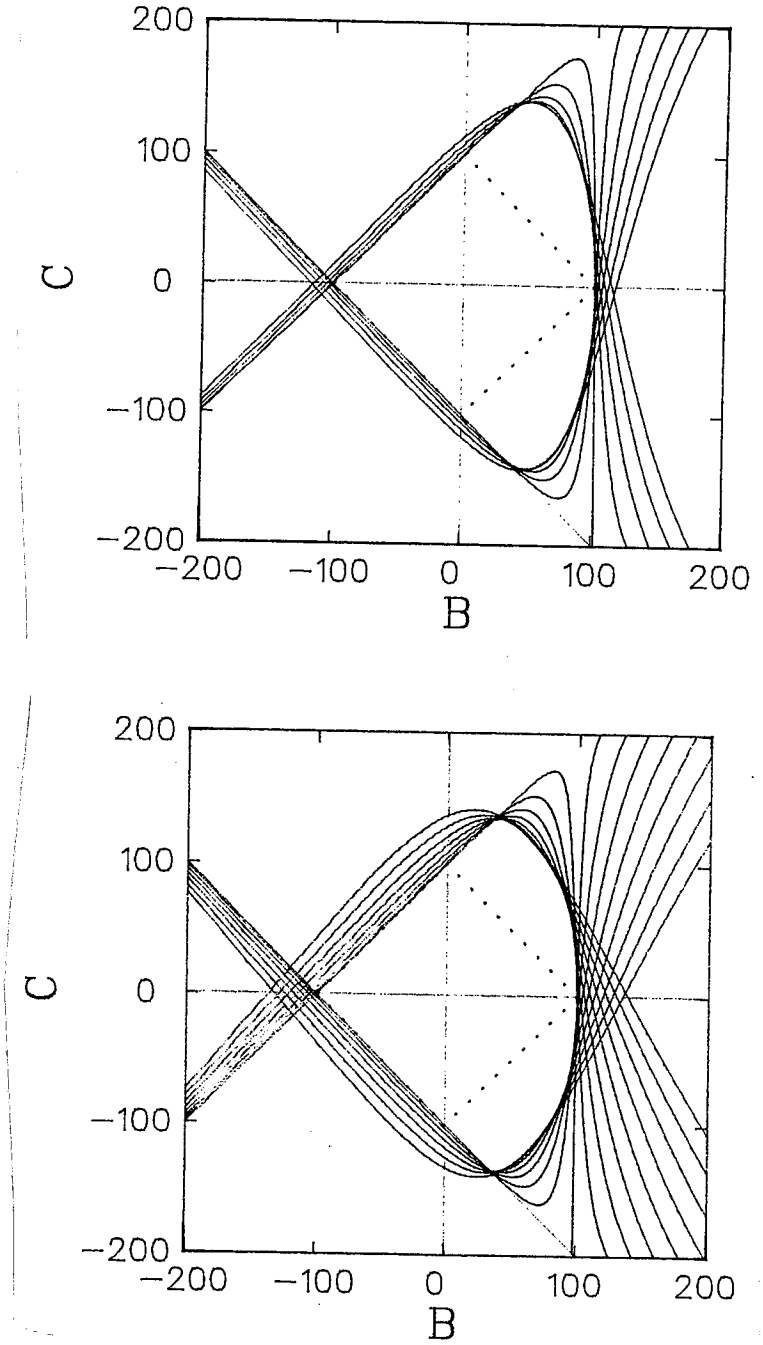

Figure 7.1: The top figure shows a cross-section of the BC-plane at $A = 100$ for $R = 0.5$ with the first 10 bifurcation surfaces bounding the stability region. The bottom figure is a similar cross-section for $R = 0.49$ with the first 16 bifurcation surfaces bounding the stability region.

region to the delay R as A changes.

We conjecture that the large area of stability beyond the MRS for $R = 0.5$ is primarily due to the small number of bifurcation curve families (in this case two). The high degree of familial ordering with only two basic shapes prevents the bifurcation curves from asymptotically approaching the MRS. It is less clear why the basic shape of the region of stability remains the same, increasing proportionally with A. In addition, the process which preserves an almost linear relationship between the number of bifurcation curves on the boundary of the stability region and A, remains an open question. Further research is needed in these areas.

Using the discussion of curve periodicity in Section 3, we find that there are 102 bifurcation curve families for $R = 0.49$. Nevertheless, the shape and organization of the bifurcation curves in Figs. 7.1 and 7.2 for $R = 0.49$ are similar to the two families of $R = 0.5$. The bifurcation curves for $R = 0.49$ drift in a counterclockwise direction clustering into what appears to be a four families structure. As A increases and more bifurcation curves are added to the boundary of the stability region, the bifurcation curves for $R = 0.49$ asymptotically approach the MRS, departing from the geometry of two family structure of $R = 0.5$. We conjecture that the familial ordering of the bifurcation curves will restrict the asymptotic approach of $R = 0.49$ from reaching the MRS, though this has not yet been demonstrated. In practical applications, the region of stability for $R = 0.49$ can be considered asymptotically coincident with the MRS.

It is both the family structure and orientation of bifurcation surfaces that determine the asymptotic shape of the stability region for a given delay R. As a measure of the asymptotic approach of the region of stability to the MRS, we define the *bulge ratio*, $br(A) = X/Y$, where X is the maximum distance between the boundary of the region of stability and either of the lines $B + C = 0$ or $B - C = 0$ and $Y = A/\sqrt{2}$ is the distance between the boundary of the MRS and either of the aforementioned lines. The bulge ratio gauges variations in the size of the stability region relative to the MRS as the parameters A and R are changed.

In the previous sections, we demonstrated that transitions cause local distortions in the shape of the stability region, often adding significantly to the volume of the stability surface. Asymptotically, transitions remain important in determining the size of the stability region and the rate at which it appoaches the MRS. Ignoring any contribution from stable spurs, we observe that the maximum distention of the stability region at the A_j^*

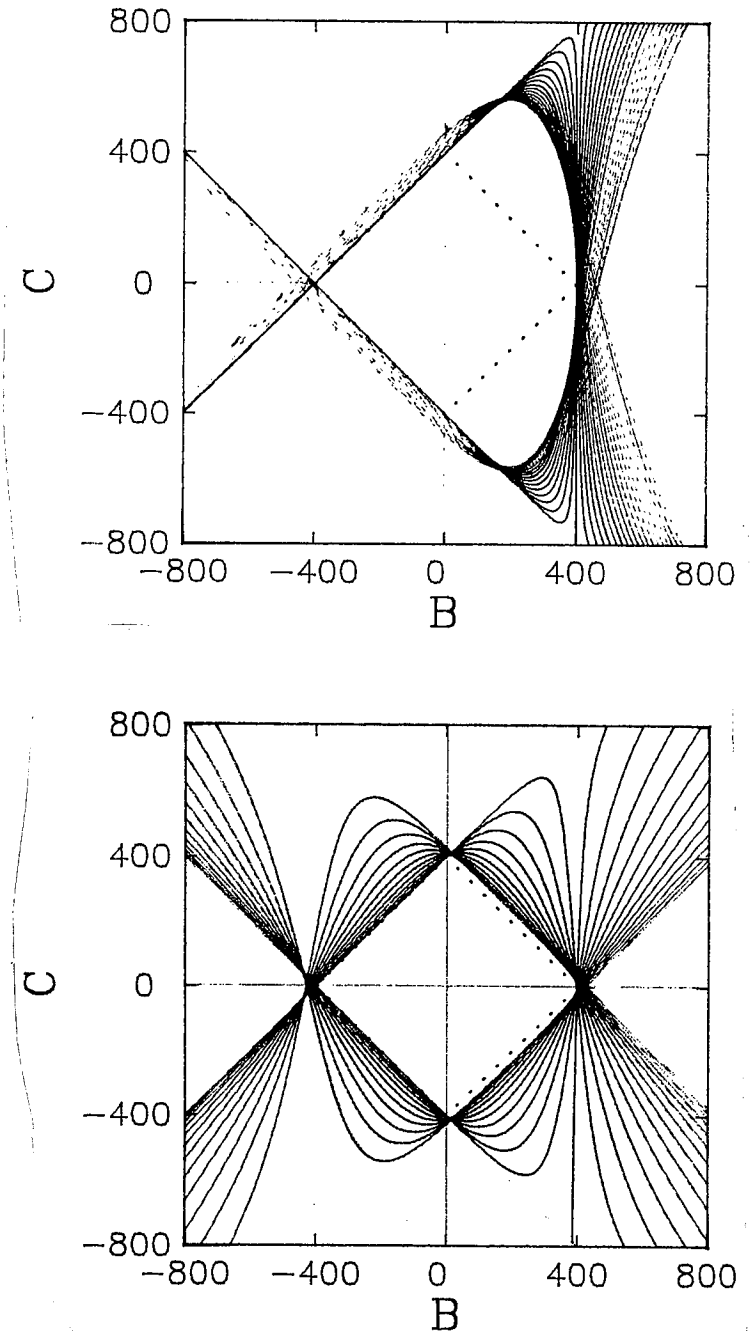

Figure 7.2: The top figure shows a cross-section of the BC-plane at $A = 400$ for $R = 0.5$ with the first 38 bifurcation surfaces bounding the stability region. The bottom figure is a similar cross-section for $R = 0.49$ with the first 26 bifurcation surfaces bounding the stability region.

transition occurs at (B_j^*, C_j^*). (For example, see Fig. 4.3 and Fig. 5.3.) At A_j^*, Eqns. (3.8) and (3.10) can be used to find the bulge ratio,

$$\begin{aligned} br(A_j^*) &= \frac{|B_j^* - (-1)^j C_j^*|}{A_j^*} \\ &= \left| \left[\frac{(1+R)}{(1-R)} \sec\left(\tfrac{j\pi}{1-R}\right) - \frac{2}{j\pi} \sin\left(\tfrac{j\pi}{1-R}\right) \right] \right|. \end{aligned} \tag{7.1}$$

This equation proves useful in examining the asymptotic properties of the stability region.

First we analyze the sensitivity of the bulge ratio to changes in A for several delays near $R = 0.5$. The results for $5 \leq A \leq 500$ are shown in Fig. 7.3. The case $R = 0.5$ is clearly an anomaly with its bulge ratio rapidly approaching a limit of two. That is, there is always a point on the boundary of the stability region that remains at least twice as far from the lines $B + C = 0$ or $B - C = 0$ as is the MRS. The other delays shown in Fig. 7.3 have bulge ratios similar to $R = 0.5$ for moderate values of A as expected by continuity of (3.2), but their bulge ratios peak near three at A_1^*. (Recall that $A_1^* = +\infty$ for $R = 0.5$.) Eqn. (7.1) can be used to verify that $br(A_1^*) \to 3$ as R increases to 0.5. For the delays studied near $R = 0.5$, there are other transitions outside the stability region prior to A_1^*. As a result, for $A > A_1^*$ many of the bifurcation curves for these delays are oriented differently from the bifurcation curves for $R = 0.5$. In this way, the stability region for $R < 0.5$ and $A > A_1^*$ diverges from the special case $R = 0.5$, with the stability region for these delays appearing to approach the MRS for large A.

The analysis above identifies two factors contributing to the unusually large region of stability for $R = 0.5$. First, the two families of bifurcation curves do not permit sufficient geometric variation for the stability region to approach the MRS. Second, given any $\tilde{A} > 0$ there exists some $R \in (\frac{1}{3}, \frac{1}{2})$ with $\tilde{A} = A_1^*$, which from (7.1) satisfies $br(\tilde{A}) > 3$. When $A > A_1^*$ for $R < \frac{1}{2}$, the bifurcation curves have a different orientation, and the bulge ratio decreases as the two family ordering disappears. It is the confluence of these factors that keeps the stability surface bounded away from the MRS when $R = \frac{1}{2}$ for all A, with its cross-sectional shape resembling the one pictured in Fig. 7.2 for large A.

A similar argument can be made for several other specific delays. The delays $R = \frac{1}{3}$ and $R = \frac{1}{4}$ follow $R = \frac{1}{2}$ in having the smallest number of bifurcation curve families with four and six, respectively. Fig. 7.4 presents

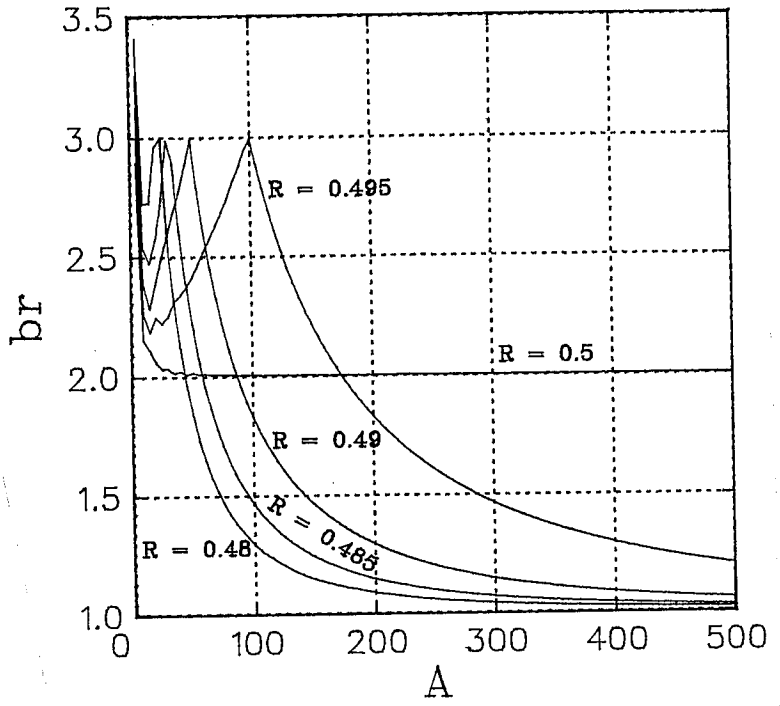

Figure 7.3: Graph of the bulge ratio versus A for several delays near $R = 0.5$.

cross-sections of the stability region at $A = 400$ for $R = \frac{1}{3}$ and $R = \frac{1}{4}$ showing the organization of the families of bifurcation curves. These figures only present the bifurcation curves that have an impact on the boundary of the stability region. For $R = \frac{1}{3}$, the boundary is comprised of the first bifurcation curve, the second family $(2, 6, 10, \ldots)$, and the fourth family $(4, 8, 12, \ldots)$; while for $R = \frac{1}{4}$, the first bifurcation curve, the third family $(3, 9, 15, \ldots)$, and the sixth family $(6, 12, \ldots)$ create the boundary of the stability region. As in the case $R = \frac{1}{2}$, the construction of the stability region boundary is dominanted by two families for both $R = \frac{1}{3}$ and $R = \frac{1}{4}$. Numerical studies show that the bulge ratio for $R = \frac{1}{3}$ tends to 1.414 as A becomes large, with its stability area about 26.6% larger than the MRS. For $R = \frac{1}{4}$, the bulge ratio tends to 1.237, and numerical integration yields a stability area about 14.7% larger than the MRS.

In each of the aforementioned cases, transitions appear to affect the

size of the stability region asymptotically in A. From (3.8) it follows that $A_2^* \to +\infty$ as R increases to $\frac{1}{3}$. Equation (7.1) can be used to show that $br(A_2^*) \to 2$ as R increases to $\frac{1}{3}$. Similarly, as R increases to $\frac{1}{4}$, $A_3^* \to +\infty$ and $br(A_3^*) \to 1.667$. As was seen for $R = \frac{1}{2}$, the transitions A_2^* and A_3^* create distentions in the boundary of the stability region for R near $\frac{1}{3}$ and $\frac{1}{4}$ with this local bulge occurring for higher values of A as R increases to either $\frac{1}{3}$ or $\frac{1}{4}$. Thus, the highly structured ordering of the bifurcation curves and the effects of the transitions described above appear to prevent the stability regions for $R = \frac{1}{3}$ and $\frac{1}{4}$ from asymptotically approaching the MRS.

When $R = \frac{1}{5}, \frac{1}{6}$, or $\frac{1}{7}$, the bifurcation curves again organize into a small number of highly ordered families of which only two families along with the first bifurcation curve are on the boundary of the stability region for A sufficiently large. The bulge ratios for $R = \frac{1}{5}, \frac{1}{6}$, and $\frac{1}{7}$ tend to 1.155, 1.111, and 1.084, respectively, with stability areas 9.41%, 6.57%, and 4.90% larger than their respective MRS. As in the previous cases, the transitions A_{n-1}^* result in local distortions in the stability regions for R less than but near $\frac{1}{n}$, with the bulge ratio at the transition from (7.1) given by $br(A_{n-1}^*)$, which is decreasing in n. Again, it appears that the peak in the bulge ratio due to these transitions and the highly ordered curve families prevent the stability regions of these rational delays from asymptotically approaching the MRS.

A numerical study of the bulge ratio versus R at $A = 1000$ is presented in Fig. 7.5, where computation of the bulge ratio is undertaken at intervals of $R = 0.002$. If data were collected continuously in R for Fig. 7.5, then as R increased, the bulge ratio would increase to about three for $\tilde{R} \simeq 0.4995$ (since $A_1^*(\tilde{R}) = 1000$), and subsequently decrease to about two when $R = \frac{1}{2}$, which is the largest value that appears in the figure. Because of the grid generating the data points, many of the peaks caused by transitions are lost in the figure. The graph in Fig. 7.5 shows the largest asymptotic bulge ratios in descending order are $R = \frac{1}{2}, \frac{1}{3}, \frac{1}{4}, \frac{1}{5}$ and $\frac{1}{6}$, each of which was discussed above. In fact, at $A = 1000$ there are transitions just prior to each of these values of R resulting in bulge ratios which exceed those for $R = \frac{1}{n}$. As noted above this is a local phenomenon, so that as A increases the bulge ratio peak due to the transition A_{n-1}^* occurs at R values closer to $\frac{1}{n}$, with transition peak heights nearly constant.

One interesting peak that appears in Fig. 7.5 and was not discussed above is the one at $R = \frac{2}{5}$. The asymptotic bulge ratio approaches 1.110 with a stability region that is 7.17% larger than the MRS. From Section 3, we find that $R = \frac{2}{5}$ has only six families of bifurcation curves, the same number as $R = \frac{1}{4}$, yet its asymptotic bulge ratio is significantly lower. The variation

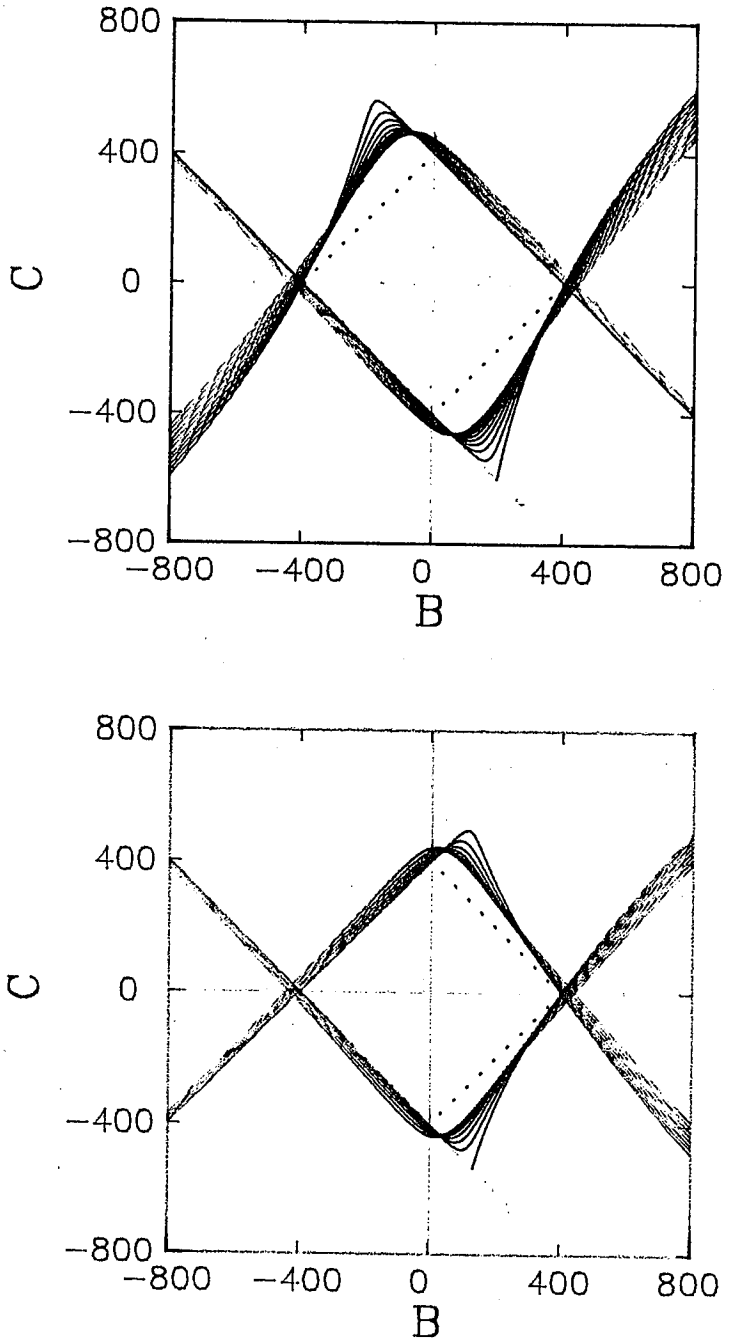

Figure 7.4: The top figure shows the cross-section of the stability region for $R = \frac{1}{3}$ when $A = 400$, while the bottom figure shows the cross-section of the stability region for $R = \frac{1}{4}$ when $A = 400$. The top figure requires a collection of the first 44 bifurcation curves, while the bottom figure requires some of the first 45 bifurcation curves to construct the boundary of its stability region.

in bulge ratios is due in part to differences in the organization of bifurcation families on the boundary of the stability region between $R = \frac{2}{5}$ and $R = \frac{1}{4}$. We note that for delays near $R = \frac{2}{5}$ there are no transitions for bifurcation curves on the boundary of the stability region. This demonstrates the importance of both the structure of the bifurcation curves families and the set of transitions on the stability region boundary in determining the asymptotic bulge ratio. Additional work is needed on problems of this type.

Extending the reasoning given in this section for specific rational delays in the interval $(0, \frac{1}{2})$, we consider any delay, rational or irrational, over the same interval. Since all rational delays have a finite number of bifurcation curve families, we conjecture that rational delays will have stability regions larger than the MRS though generally the deviation will be quite small asymptotically. If the delay, R, is irrational, by Section 3 it will have no families of bifurcation curves. Without a specific curve ordering from families of bifurcation curves, we conjecture that irrational delays will have stability regions which are asymptotically coincident with the MRS.

8 Discussion

Our work has outlined a methodology for identifying and characterizing the stability region in the coefficient parameter space of the two delay differential equation given by (3.1) when $R \leq \frac{1}{2}$. For most delays, the stability region begins at a specific point given by Theorem 3.2, which is easily seen in the 3-dimensional figures, and is bounded by part of the first bifurcation surface and the $A + B + C = 0$ plane. Along the former a Hopf bifurcation occurs, while the latter exhibits a loss of stability as a real root crosses the imaginary axis in the eigenspace. Increasing the coefficient of the undelayed term, A, we discovered only a limited number of ways in which changes to the boundary of the stability region occur.

The most significant changes resulted from transitions, A_j^*. If the j^{th} bifurcation surface is part of the boundary of the stability region when $A < A_j^*$, then at A_j^*, there is a degeneracy as two bifurcation curves meet at a point, and a Hopf bifurcation occurs with eigenvalues $\lambda = \pm\frac{j\pi}{1-R}i$ along part of the line given by (3.10). At the transition a stable spur from the self-intersection of the $j + 1^{\text{st}}$ bifurcation surface joins the stability region. Subsequently, the $j + 1^{\text{st}}$ bifurcation surface enters the boundary of the stability region. At a transition the asymptotic limits of the two bifurcation

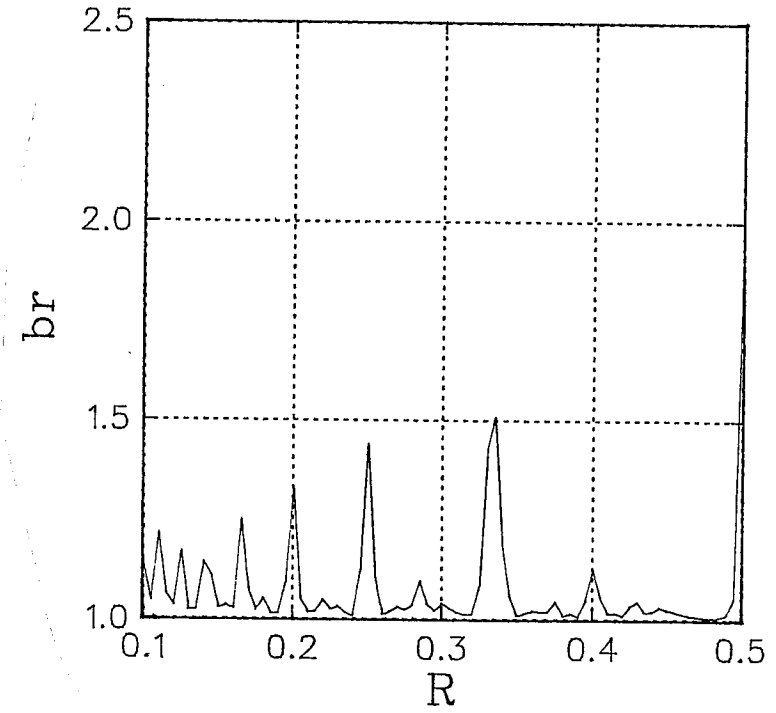

Figure 7.5: Graph of the bulge ratio versus R at $A = 1000$.

surfaces involved swap positions, causing a major distortion in the boundary of the stability region.

For $R \leq \frac{1}{2}$, we observed only two other ways in which new bifurcation surfaces could enter the boundary of the stability region, transferrals and tangencies, as defined in Section 3 and illustrated in Section 4. By studying how the bifurcation surfaces could enter the boundary of the stability region, we were able to develop numerical methods to trace when a transition, transferral, or tangency affected the boundary for a given value of R. With this information we generated the complete stability region for bounded values of A over a range of R values. In Section 5, we presented a series of 3-dimensional plots showing how the stability regions vary with R, often observing significant changes when R is perturbed slightly. In Section 6, we provided information for finding the boundary of the stability region when $R \in (0, \frac{1}{2}]$. In addition, we demonstrated the significance of transitions and

their associated stable spurs as R decreases. Our analysis shows that the shape and size of the stability region is very sensitive to changes in the parameters, especially R.

One picture that emerged from our analyses was the difference in the regions of stability for low order fractional delays such as $\frac{1}{2}$ and $\frac{1}{3}$. These delays exhibit atypically large stability regions which persist as $A \to \infty$. We showed that near these fractional delays there is an accumulation of transitions that distort the regions of stability of delays nearby (for example, compare Figs. 5.7 and 5.8). In Section 7, we performed a series of numerical experiments to demonstrate how much larger the regions of stability were for certain delays. For most delays as A increased, the region of stability rapidly approached the Minimum Region of Stability given in Theorem 3.1. However, when $R = \frac{1}{2}$, the region of stability remained almost 68% larger than the MRS. Other delays such as $\frac{1}{3}$ and $\frac{1}{4}$ also have enlarged stability regions, which seem to reflect the dominant effects that transitions have in determining the stability region. Thus, the size of the stability region can be very sensitive to variations in R. This sensitivity to variations in R should be recognized when characterizing stability properties of a mathematical model with two delays.

This paper answers many questions on the complicated nature of the stability of (3.1). Yet, there are many questions that remain to be addressed. We limited this work to the range of $R \leq \frac{1}{2}$ since the bifurcation curves are simpler. Over this range the bifurcation curves rarely self-intersect which is not the case when $R > \frac{1}{2}$. We have noted that transitions create the most significant changes in the region of stability and observed that as $R \to 0$ transitions occur more frequently with larger stable spurs. More studies are needed for small values of R. Our studies on the asymptotic limits as $A \to \infty$ in Section 7 were primarily numerical, so additional analytical work should be performed. Nevertheless, our results provide a framework for studying applications utilizing differential equations with two delays.

A Appendix: D-Decomposition Partitions

This appendix identifies the region of stability for (3.1) by applying the D-decomposition method discussed in El'sgol'ts [7]. The image of the imaginary axis for (3.2) is a countable set of curves in the BC-plane for each value of A and comprises the boundary of the D-decomposition partitions. When $R < \frac{1}{2}$ all of these curves are simple, except when a stable spur forms. Crossing a bifurcation curve results in the gain or loss of two eigenvalues with positive real part. The D-decomposition method uses this information to determine the number of eigenvalues with positive real part in each portion of the BC-plane partitioned by the bifurcation curves. Fig. A.1 diagrams a cross-section in BC-space of the first bifurcation surface when $R = \frac{1}{3}$ and $A = -2$, which is near the initial point of Theorem 3.2.

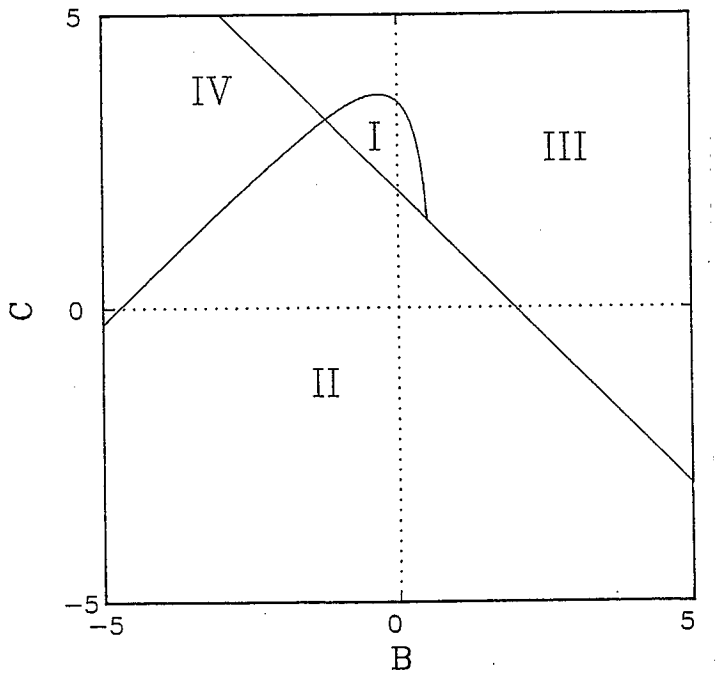

Figure A.1: Example illustrating the D-decomposition method. Shown is the case where $R = \frac{1}{3}$ and $A = -2$.

The line in Fig. A.1 is the projection of the $A + B + C = 0$ plane where a real root of (3.2) occurs. The other curve in the figure is generated from (3.4) as the parameter ω increases from 0, showing part of the first bifurcation

surface. The range shown in Fig. A.1 is sufficiently restricted so that it does not include any additional images of the imaginary axis, i.e., the other bifurcation surfaces lie outside the region shown. Crossing the projection of the $A+B+C=0$ plane to the left or down creates a real positive root, while crossing the curve projecting the first bifurcation surface into either Region III or IV generates two complex conjugate roots of (3.2) with positive real parts. Thus, Regions II, III, and IV have one, two, and three roots of (3.2) with positive real parts, respectively, and Region I is the region of stability with all solutions of (3.2) having roots with negative real parts.

Equation (3.5) gives the initial point at which the first bifurcation surface and the $A+B+C=0$ plane coincide as $\omega \to 0$. To show that the first bifurcation surface proceeds above the plane as seen in Fig. A.1, we must demonstrate that $B+C > -A$ for B and C given by (3.4) and ω slightly greater than zero. This is equivalent to

$$A(\sin\omega R - \sin\omega) + \omega(\cos\omega R - \cos\omega) > -A\sin(\omega(1-R)).$$

By taking the first two terms of the Maclaurin series expansion for the sine and cosine functions and dropping higher order terms, the above expression reduces to $A > -(R+1)/R \equiv A_0$. Thus, for $A > A_0$, the first bifurcation surface begins by rising above the $A+B+C=0$ plane. To complete the proof that the first bifurcation curve is as pictured in Fig. A.1, we must show that it returns to intersect the $A+B+C=0$ plane. However, until $A = A_1^*$, we see that $(B(\omega), C(\omega)) \to (-\infty, -\infty)$ as $\omega \to (\frac{\pi}{1-R})^-$, which implies that the first bifurcation curve intersects the $A+B+C=0$ plane a second time. Therefore, the boundary of the stability region in the BC-plane is circumscribed by the first bifurcation curve and the $A+B+C=0$ plane for some range of $A > A_0$ (assuming there are no stable spurs in this cross-section).

The 2-dimensional analysis on the BC-cross-sections extends easily to the 3-dimensional ABC-parameter space. The bifurcation surfaces defined in Section 3 form boundaries that partition the 3-dimensional parameter space into regions with the same number of eigenvalues with positive real part. By carefully following changes in the boundaries of the BC-cross-sections, the 3-dimensional structure of the stability region (no eigenvalues with positive real part) is found as A varies. This is shown to be a connected set in our geometrical analysis.

B Appendix: The Transistion A_1^* and The Existence of Stable Spurs

Theorem 3.2 provides the initial point of the bifurcation surface over a range of the delay R. As A increases, the first bifurcation surface and the $A+B+C=0$ plane bound the stability region in the BC cross-sections as seen in Fig. A.1. In this appendix we show that for $R<\frac{1}{2}$, there is a transitional value, A_1^*, given by (3.8). For $A>A_1^*$ at least one additional bifurcation surface bounds the stability region, which differs from the one delay problem. Prior to the transition at A_1^*, the second bifurcation curve self-intersects capturing a region of stability distinct from that given by Theorem 3.2. The collection of these BC cross-sections join the principal region of stability at A_1^*, forming what we define as a stable spur. Furthermore, every transition on the boundary of the stability region has an associated stable spur.

When $R<\frac{1}{2}$ and $A<A_1^*$, (3.4) shows that

$$\lim_{\omega\to(\frac{\pi}{1-R})^-}(B(\omega),C(\omega))=(-\infty,-\infty);$$

while for $A>A_1^*$,

$$\lim_{\omega\to(\frac{\pi}{1-R})^-}(B(\omega),C(\omega))=(+\infty,+\infty).$$

This demonstrates a dramatic change in the first bifurcation surface and indicates that a transition occurs at A_1^*. In particular, when $A=A_1^*$ and $\omega=\frac{\pi}{1-R}$, the real part of (3.3) is zero for any B and C. The imaginary part of (3.3) is satisfied when:

$$B-C=\frac{\pi}{1-R}\csc\left(\tfrac{\pi}{1-R}\right), \tag{B.1}$$

which generates a line in the BC-plane at $A=A_1^*$. As $\omega\to\frac{\pi}{1-R}$, Eqn. (3.9) with $j=1$ gives the value of the point (B_1^*,C_1^*) where the first bifurcation curve terminates and the second bifurcation curve begins. The line given by (B.1) becomes a boundary in the D-decomposition partition of the space at $A=A_1^*$. (See Fig. 4.3 as a representative cross-section of this transition.) Below (B_1^*,C_1^*) there are two more eigenvalues with positive real part above (B.1) than below this line, while above (B_1^*,C_1^*) there are two fewer eigenvalues when passing from below (B.1) to above this line.

The graph in Fig. 6.1 shows that $A_0 < A_1^*$ for all $0 < R < \frac{1}{2}$. For $\frac{1}{3} \leq R < \frac{1}{2}$, it is clear that $A_0 < A_1^*$ as $A_0 < 0$ and $A_1^* \geq 0$. The expression $A_0 < A_1^*$ is equivalent to

$$\cos\left(\tfrac{R\pi}{1-R}\right) < \frac{1-R^2}{R\pi}\sin\left(\tfrac{R\pi}{1-R}\right). \tag{B.2}$$

For small R, the Maclaurin series expansion for cosine and sine readily verify this inequality. Let $x = \frac{R\pi}{1-R}$, then (B.2) can be written

$$x\cos x < (1+R)\sin x, \quad 0 < x < \frac{\pi}{2}.$$

The derivative of $x\cos x$ is less than $\cos x$ for $0 < x < \frac{\pi}{2}$ which demonstrates that (B.2) is valid for $0 < R < \frac{1}{3}$ and proves that $A_0 < A_1^*$ for all $0 < R < \frac{1}{2}$. It is easy to see that $A_1^* \to \infty$ as $R \to \frac{1}{2}$.

For $R \leq \frac{1}{2}$, the bifurcation curves generated by (3.4) are usually simple curves in the BC-plane. An exception is seen in Fig. 4.2, where a loop develops in the second bifurcation curve. Fig. 4.5 shows the 3-dimensional stable spur that results as the 2-dimensional cross-sections of loops in the second bifurcation curve grow from a point at A_1^p and join the principal region of stability at the transition value, A_1^*. Below, an algorithm is provided for computing the initial point of the stable spur at a given transition value of A for any $R \in (0, \frac{1}{2})$.

Fig. 4.6 depicts a typical cross-section of bifurcation curves in which $C(\omega)$ is monotone for the first and third families of curves. In the second and fourth families, $C(\omega)$ has a single extremum. That is, the equation $dC/d\omega = 0$ has no solutions for the first and third families and only one solution for the second and fourth families. This schema breaks down when considering the second bifurcation curve in Fig. 4.2, which shows that $dC/d\omega = 0$ has two solutions. Specifically, we find that the second bifurcation curve is monotone in C until $A = A_1^p$, then it has two extrema for $A \in (A_1^p, A_1^*)$. For $A > A_1^*$, there is another extremum at which C reaches its maximum value and the second bifurcation curve is again simple.

Using (3.4), we can compute $dC/d\omega$:

$$\begin{aligned}\frac{dC}{d\omega} &= \frac{-\sin(\omega(1-R))[A\cos\omega + \cos\omega - \omega\sin\omega]}{\sin^2(\omega(1-R))} \\ &\quad + \frac{(1-R)\cos(\omega(1-R))[A\sin\omega + \omega\cos\omega]}{\sin^2(\omega(1-R))}.\end{aligned}$$

Using basic trigonometric identities on the numerator of this expression, we define the following function:

$$\text{(B.3)} \quad f(\omega) \equiv \tfrac{1}{2}\Big([A(2-R)+1]\sin\omega R - (AR+1)\sin\omega(2-R) + \omega(2-R)\cos\omega R - \omega R\cos\omega(2-R)\Big).$$

Note that the function f also depends on the parameters A and R. Computing $dC/d\omega = 0$ is equivalent to $f(\omega) = 0$. To study the zeroes of f, its derivative is needed and is given by:

$$\text{(B.4)} \quad f'(\omega) = \Big([AR(2-R)+2]\sin\omega + \omega R(2-R)\cos\omega\Big)\sin\omega(1-R).$$

When $f'(\omega) = 0$, we can solve (B.4) to yield:

$$\text{(B.5)} \qquad \tan\omega = -\frac{\omega R(2-R)}{AR(2-R)+2}.$$

The length of the interval for the j^{th} bifurcation curve is $\frac{\pi}{1-R}$. Since $R \in (0, \frac{1}{2}]$, this interval has a length between π and 2π. For any given bifurcation curve the number of solutions to (B.5) is either one or two, which implies that $f(\omega)$ has either one or two extrema. Next we examine the endpoints of the j^{th} bifurcation curve.

Let $\omega = \frac{j\pi}{1-R}$, then (B.3) gives:

$$\text{(B.6)} \quad \begin{aligned} f(\tfrac{j\pi}{1-R}) &= A(1-R)(-1)^j \sin\tfrac{j\pi}{1-R} + j\pi(-1)^j\cos\tfrac{j\pi}{1-R}, \\ &= \begin{cases} (-1)^j(A-A_j^*)(1-R)\sin\frac{j\pi}{1-R}, & \frac{j}{1-R} \notin Z, \\ (-1)^j j\pi\cos\frac{j\pi}{1-R}, & \frac{j}{1-R} \in Z, \end{cases} \end{aligned},$$

where $A_j^* = -\frac{j\pi}{1-R}\cot\frac{j\pi}{1-R}$ is the j^{th} transition. To simplify our discussion we concentrate our analysis on the first stable spur which arises from the second bifurcation curve with A slightly less than A_1^*. Finding the other stable spurs uses very similar techniques. For the first stable spur we examine

$$f(\tfrac{\pi}{1-R}) = (A_1^* - A)(1-R)\sin\tfrac{\pi}{1-R}$$

and

$$f(\tfrac{2\pi}{1-R}) = \begin{cases} (A-A_2^*)(1-R)\sin\frac{2\pi}{1-R}, & R \neq \frac{1}{3}, \\ -2\pi, & R = \frac{1}{3}, \end{cases}.$$

Since $\sin\frac{\pi}{1-R} < 0$ for $R \in (0, \frac{1}{2})$, $f(\frac{\pi}{1-R})$ is negative if $A < A_1^*$ and positive if $A > A_1^*$. For A near A_1^*, it can be shown that $f(\frac{2\pi}{1-R}) < 0$ as $A_1^* < A_2^*$ for $0 < R < \frac{1}{3}$ and $A_1^* > A_2^*$ for $\frac{1}{3} < R < \frac{1}{2}$.

From (B.4) it is easy to see that $f'(\omega) = 0$ at $\omega = \frac{j\pi}{1-R}$. Consider $f'(\omega)$ in a neighborhood of the endpoints. Let $\omega = \frac{\pi^+}{1-R}$ be a point near the initial ω value for the second bifurcation curve, then

$$\begin{aligned} f'(\tfrac{\pi^+}{1-R}) &= \left(AR(2-R)+2\right)\sin\tfrac{\pi^+}{1-R} + \tfrac{\pi^+}{1-R}R(2-R)\cos\tfrac{\pi^+}{1-R}\Big)\sin\pi^+, \\ &\simeq \left[(A-A_1^*)R(2-R)\sin\tfrac{\pi^+}{1-R} + 2\sin\tfrac{\pi^+}{1-R}\right]\sin\pi^+. \end{aligned}$$

For $A - A_1^* < R(2-R)/2$, this expression is positive for a range of $\omega > \frac{\pi}{1-R}$. Near the other endpoint we examine a point $\omega = \frac{2\pi^-}{1-R}$. The expression

$$f'(\tfrac{2\pi^-}{1-R}) \simeq \left[(A-A_2^*)R(2-R)\sin\tfrac{2\pi^-}{1-R} + 2\sin\tfrac{2\pi^-}{1-R}\right]\sin 2\pi^-$$

is positive for $|A_2^* - A| > R(2-R)/2$ and A near A_1^*.

The above information shows that if A is sufficiently close to A_1^*, then the graph of f begins by increasing to some maximum, then decreasing to a minimum, after which it increases and obtains a negative value for $f(\frac{2\pi}{1-R})$. When A is farther from A_1^*, one of these extrema might disappear or the final endpoint might not be negative. There is a range of A with $A < A_1^*$ such that f remains negative for all $\omega \in [\frac{\pi}{1-R}, \frac{2\pi}{1-R}]$, or equivalently, the second bifurcation curve is monotonically decreasing in C. As A increases to $A_1^p < A_1^*$, there exists an ω_p with $f(\omega_p) = f'(\omega_p) = 0$, where the stable spur begins. For $A \in (A_1^p, A_1^*)$, the graph of f for $\omega \in [\frac{\pi}{1-R}, \frac{2\pi}{1-R}]$ begins negative, then increases to a positive maximum before ending with a negative value. Thus, $dC/d\omega$ has two roots in this interval which causes a loop in the second bifurcation curve. For $A > A_1^*$ (yet sufficiently close), the graph of f starts positive, then becomes negative, which indicates that the second bifurcation curve increases to a maximum and then decreases as pictured in Fig. 4.6. Thus, our calculations show that there is always a stable spur at a transition for $R < \frac{1}{2}$.

To find the initial point of a stable spur for any R and j, an algorithm was developed that solved (B.3) and (B.4) simultaneously equal to zero for ω and the parameter A. The value $A = A_j^p$ determines where the stable spur begins, and $\omega = \omega_j^p$ gives the frequency of the bifurcation at this point. The numerics lead to several observations. First, the $(j+1)^{\text{st}}$ stable spur is shorter than the j^{th} for any given R. Secondly, the length of the stable

spur increases with decreasing R. Thus, A_1^p is the beginning of any stability region generated by stable spurs. Numerically, we find that $A_1^p < A_0$ for $R \leq 0.0016$. This implies that as A increases, the stable spur, bounded solely by the second bifurcation curve, forms the first region of stability. Subsequently, another region of stability emanates from A_0 and is bounded by the first bifurcation curve and the $A + B + C = 0$ plane. We have not conducted studies for these small delays, so the significance of stable spurs in this region is unknown. For $R > R_0 \equiv 0.0017$, the stability region begins at A_0 and is summarized in Theorem 3.2.

C Appendix: Detailed Curve Analysis for $R = \frac{1}{3}$

The bifurcation curves shown in Fig. 4.5 with $R = \frac{1}{3}$ have four characteristic shapes and a periodic curve ordering which partitions the curves into four families, as discussed in the text. This distinct ordering facilitates the construction of the stability region.

In this section, a detailed analysis of the shapes of the curves that comprise the four families shown in Fig. 4.5 is undertaken. A rotation of 45° will simplify the analysis of the families of curves, so we introduce the following change of coordinates:

$$\begin{aligned} X &= B + C = \frac{-A\cos\left(\frac{\omega(1+R)}{2}\right) + \omega\sin\left(\frac{\omega(1+R)}{2}\right)}{\cos\left(\frac{\omega(1-R)}{2}\right)}, \\ Y &= B - C = \frac{A\sin\left(\frac{\omega(1+R)}{2}\right) + \omega\cos\left(\frac{\omega(1+R)}{2}\right)}{\sin\left(\frac{\omega(1-R)}{2}\right)}. \end{aligned} \tag{C.1}$$

These equations are derived from (3.4) after some trigonometric simplifications. With $R = \frac{1}{3}$, Eqn. (C.1) yields:

$$\begin{aligned} X &= \frac{-A\cos\left(\frac{2\omega}{3}\right) + \omega\sin\left(\frac{2\omega}{3}\right)}{\cos\left(\frac{\omega}{3}\right)}, \\ Y &= \frac{A\sin\left(\frac{2\omega}{3}\right) + \omega\cos\left(\frac{2\omega}{3}\right)}{\sin\left(\frac{\omega}{3}\right)}. \end{aligned} \tag{C.2}$$

The equations given in (C.2) allow us to obtain analytical results for the bifurcation curve families. To prove certain results, the slope of the curves in the rotated coordinate system are required. Maple^{TM} was used to compute the following:

$$\frac{dY}{dX} = \frac{\left(2A\sin^3\frac{\omega}{3} - 3\sin\frac{\omega}{3}\cos\frac{2\omega}{3} + \omega(2\sin^2\frac{\omega}{3} + 1)\cos\frac{\omega}{3}\right)}{-A(2\cos^2\frac{\omega}{3} + 1) - 3\cos\frac{\omega}{3}\sin\frac{2\omega}{3} - 2\omega\cos^3\frac{2\omega}{3}}\cot^2\frac{\omega}{3}. \tag{C.3}$$

Fig. C.1 shows the four bifurcation curve families in the rotated coordinate system for $R = \frac{1}{3}$. The formulae above are used to show some of the properties intrafamilial members share.

Consider the first family of bifurcation curves. These curves are formed by examining $6k\pi < \omega < 6k\pi + \frac{3\pi}{2}$, $k = 0, 1, \ldots$ The following limits are

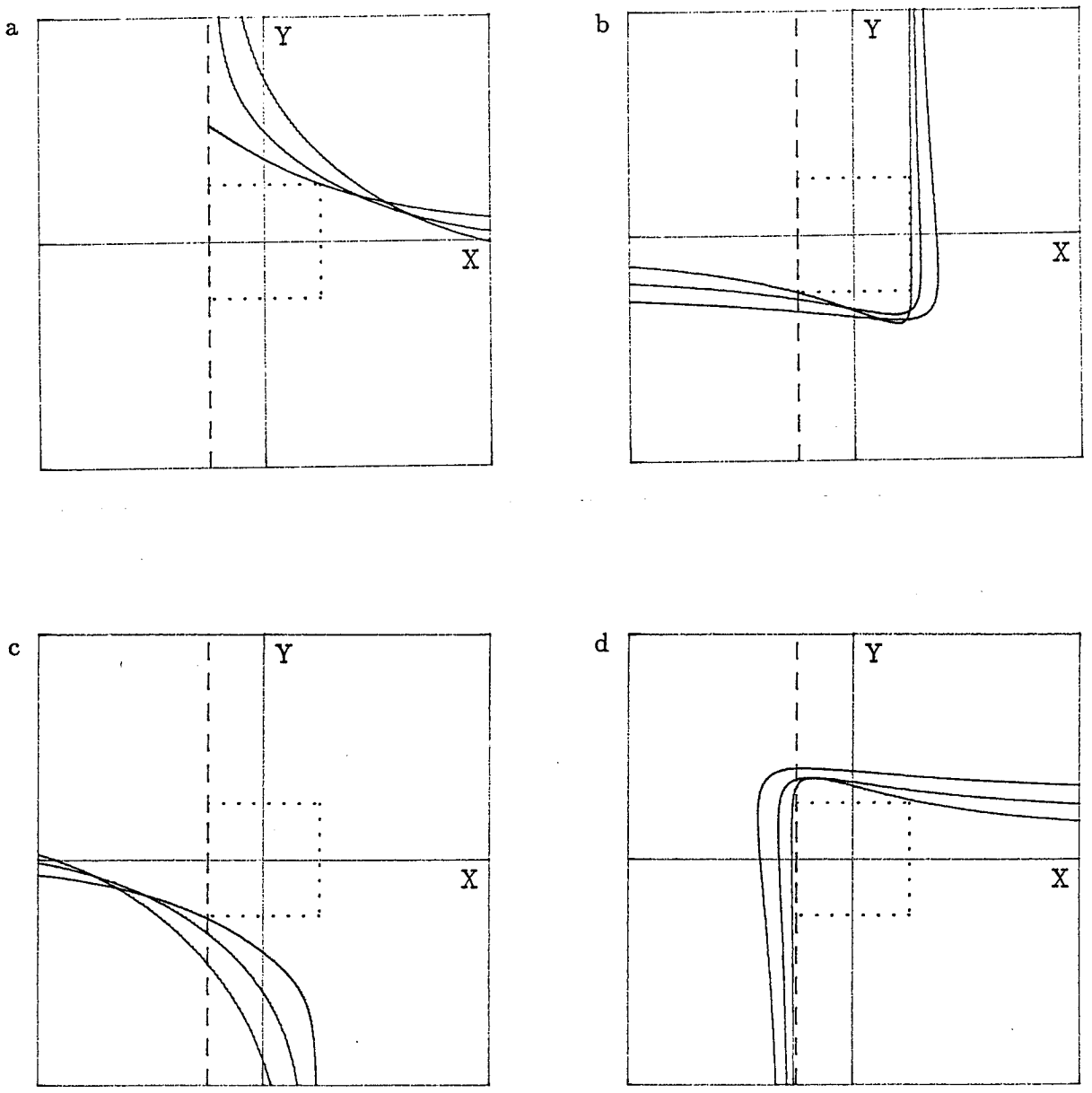

Figure C.1: The four families of bifurcation curves for $R = \frac{1}{3}$ in the rotated coordinate systems.

readily obtained from (C.2):

$$\lim_{\omega \to 6k\pi^+} X(\omega) = -A,$$

$$\lim_{\omega \to 0^+} Y(\omega) = 2A + 3, \qquad \lim_{\omega \to 6(k+1)\pi^+} Y(\omega) = +\infty, \quad k = 0, 1, ...$$

and

$$\lim_{\omega \to 6k\pi + 3\pi/2^-} X(\omega) = +\infty$$

$$\lim_{\omega \to 6k\pi + 3\pi/2^-} Y(\omega) = -6k\pi - 3\pi/2, \quad k = 0, 1, ...$$

Equation (C.3) can be used to show that $dY/dX < 0$ for $A > 0$ on the interval $6k\pi < \omega < 6k\pi + \frac{3\pi}{2}$, $k = 0, 1, ...$ This follows as the denominator is clearly negative on this interval and the numerator can be shown to be positive. The numerator is clearly positive for $6k\pi + \frac{3\pi}{4} \leq \omega < 6k\pi + \frac{3\pi}{2}$, $k = 0, 1, ...$ On the remaining interval, let $x = \frac{\omega}{3}$ and define

$$f(x) = -\sin(x)\cos(2x) + x(2\sin^2(x) + 1)\cos(x).$$

It follows that $f(0) = 0$ and $f'(x) > 0$ for $0 < x < \frac{\pi}{4}$. Thus, the numerator is positive over the desired interval, and the monotonicity of the first family of curves is shown.

From the one delay problem we know that the first bifurcation curve passes closest to the point $(X, Y) = (A, A)$. The asymptotic limits above show that each member of the first familiy must intersect the other members of this family at least once, but from the location of the first bifurcation curve this intersection requires that $X > A$. This places all members of this family except for the first bifurcation curve away from the boundary of stability. Notice that the second bifurcation curve (the leading curve of the second family) intersects the first bifurcation curve near $(X, Y) = (A, A)$. Thus, it becomes part of the boundary of the stability region for $A > A_1^*$.

A similar result can be obtained for the third family of bifurcation curves where $6k\pi + 3\pi < \omega < 6k\pi + \frac{9\pi}{2}$, $k = 0, 1, ...$ This family is nearly a reflection of the first family of bifurcation curves. The following limits are obtained from (C.2):

$$\lim_{\omega \to 6k\pi + 3\pi^+} X(\omega) = A, \qquad \lim_{\omega \to 6k\pi + 3\pi^+} Y(\omega) = -\infty, \quad k = 0, 1, ...$$

and

$$\lim_{\omega \to 6k\pi + 9\pi/2^-} X(\omega) = -\infty, \qquad \lim_{\omega \to 6k\pi + 9\pi/2^-} Y(\omega) = 6k\pi + 9\pi/2, \quad k = 0, 1, ...$$

In arguments similar to the ones for the first family of bifurcation curves, (C.3) yields $dY/dX < 0$ for $A > 0$ on the interval $6k\pi < \omega < 6k\pi + 3\pi/2$, $k = 0, 1, ...$ The monotonicity and positioning of these curves preempts them from joining the boundary of the stability region as seen in Fig. C.1c. In particular, this family lies outside the region bounded by the second bifurcation curve and the real root crossing, the $B + C = X = -A$ line.

The second and fourth families of curves are the most important in determining the boundary of the region of stability. The second family of bifurcation curves is defined on the interval $6k\pi + \frac{3\pi}{2} < \omega < 6k\pi + 3\pi$, $k = 0, 1, ...$, and satisfies the following limits:

$$\lim_{\omega \to 6k\pi + 3\pi/2^+} X(\omega) = -\infty, \qquad \lim_{\omega \to 6k\pi + 3\pi/2^+} Y(\omega) = -6k\pi - 3\pi/2, \quad k = 0, 1, ...$$

and

$$\lim_{\omega \to 6k\pi + 3\pi^-} X(\omega) = A, \qquad \lim_{\omega \to 6k\pi + 3\pi^-} Y(\omega) = +\infty, \quad k = 0, 1, ...$$

Equation (C.3) shows that as $\omega \to 6k\pi + \frac{3\pi}{2}^+$, $\frac{dY}{dX} \to 0$; while as $\omega \to 6k\pi + 3\pi^-$, $\frac{dY}{dX} \to -\infty$. Furthermore, the numerator of the leading factor in (C.3) approaches $2A + 3$ as $\omega \to 6k\pi + \frac{3\pi}{2}^+$, while it approaches $-6k\pi - 3\pi$ as $\omega \to 6k\pi + 3\pi^-$. Thus, there is one sign change in the numerator demonstrating that these bifurcation curves have $\frac{dY}{dX} = 0$ at some point in the interval. The denominator of the leading factor in (C.3) tends towards $-A$ as $\omega \to 6k\pi + \frac{3\pi}{2}^+$, while it approaches $12k\pi + 6\pi$ as $\omega \to 6k\pi + 3\pi^-$. Again there is one sign change, which in this case shows that the bifurcation curve becomes vertical and turns around. This distinctive shape is depicted in Fig. C.1b. It follows that each member of this family begins by decreasing to a minimum value of Y, then proceeds to a maximum X value before turning back and asymptotically approaching $X = A$.

We have shown that each member of the second family of bifurcation curves has an reflected "L" shape. From this geometry, more complicated intra-familial interactions can occur than are seen in either the first or third families. The second family contributes bifurcation curves to the boundary of the stability region for increasing values of A as successive curves meet in *tangencies*. In the text we noted that for $A > 30.4$, the sixth bifurcation curve enters the boundary of the stability region along with the second bifurcation curve. The 10^{th} bifurcation curve becomes tangent to the 6^{th} near $A = 80$. Thus, the second family, unlike the first or third families, has a sequence of surfaces which form the boundary of the stability region

through curve deformations which induce tangencies. Even though second family curves deform to become part of the boundary of the stability region, their characteristic shape persists.

Consider the behavior of successive curves at the Y-intercept. When $X = 0$ with $A > 0$ fixed, each bifurcation curve has a unique Y-intercept. From (C.2) it follows that

$$\text{(C.4)} \qquad Y = \frac{\omega}{\sin(\frac{\omega}{3})\cos(\frac{2\omega}{3})}, \qquad \text{where} \qquad \omega \tan(\tfrac{2\omega}{3}) = A,$$

for ω over the proper interval. For the second family of bifurcation curves, where $(6k + \frac{3}{2})\pi < \omega < (6k + 3)\pi$, (C.4) can be used to see that for k large, $\omega \to (6k + \frac{3}{2})\pi$ yielding $Y \to -(6k + \frac{3}{2})\pi$. Thus, the bifurcation curves of the second family pass through the third quadrant almost as parallel lines separated by 6π for large ω. This gives a clear ordering of the curves for ω sufficiently large separating this section of the second family curves away from the region of stability. As a result, for any fixed value of A only a finite number of second family curves are part of the boundary of the stability region.

The behavior of the tangent curves can be seen at the Y-intercept as higher numbered second family curves (6, 10, 14 ...) become tangent and then pass inside of the lower numbered curves. To see this, observe that the equation for Y in (C.4) has both its numerator and denominator increasing in ω which allows the ordering of the curves to reverse for some of the initial family members. In fact, as A increases more family members may swap positions leaving a higher bifurcation surface on the boundary of the stability region. Let $2k$ be the highest numbered bifurcation surface on the boundary of the stability region, then for large A our numerical studies indicate that $2k$ increases almost linearly with A. Furthermore, the ratio of the maximum Y-intercept to $-A$ tends to 1.299, which demonstrates the persistence of a bulge in the stability region beyond the MRS for large A. The existence of an aysmptotic bulge in the stability region is examined in detail in Section 7 of the text.

Similarly, when $Y = 0$ with $A > 0$ fixed, the unique X-intercept $\equiv X_0$ is found by solving

$$\text{(C.5)} \qquad X = \frac{\omega}{\cos(\frac{\omega}{3})\sin(\frac{2\omega}{3})}, \qquad \text{where} \qquad \omega \cot(\tfrac{2\omega}{3}) = -A,$$

with $\omega \in ((6k + \frac{3}{2})\pi, (6k + 3)\pi)$ for the second family of bifurcation curves. From (C.5) it can be shown that $X \to (6k + \frac{9}{4})\pi\sqrt{2}$ as $\omega \to (6k + \frac{9}{4})\pi$. Thus,

the bifurcation curves of the second family have an asymptotic separation of $6\pi\sqrt{2}$ along the X-axis before returning to asymptotically approach the line $X = A$ as $\omega \to (6k+3)\pi$, as was seen about the Y-intercept. Again this provides a clear ordering of the curves for ω sufficiently large. *A fortiori*, within this family only the second bifurcation curve lies on the boundary of the stability region in the first quadrant with tangencies occurring in the fourth quadrant.

An argument similar to that used for the second family can be applied to the fourth family of curves, demonstrating that this family behaves as in Fig. C.1d, mimicking the tangency and parallelism discussed above. The tangencies of the fourth family occur in the second quadrant with the curves becoming parallel to $X = -A$ as $\omega \to 6(k+1)\pi$. Fig. C.1d shows a tangency between the 4^{th} and 8^{th} surfaces enlarging of stability region.

There are three primary conclusions that can be drawn by combining the results above. First, when A is fixed only a finite number of bifurcation curves determine the boundary of the stability region. This follows from the ordering of the curves and the intra-familial intersections which can occur. Second, the region of stability is a connected set in $ABC-$parameter space. This can be seen from analysis with the D-decomposition partitions of El'sgol'ts [7]. Lastly, there is a bulge in the region of stability due to the intra-familial interactions among second and fourth families of bifurcation curves. In Section 7 of the text we report numerical results demonstrating that this bulge persists for delays other than $\frac{1}{3}$, though most delays yield stability regions that are nearly conincident with the Minimum Region of Stability for A sufficiently large.

References

[1] J. Bélair. Stability of a differential-delay equation with two time delays. In F. V. Atkinson, W. F. Langford, and A. B. Mingarelli, editors, *Oscillations, Bifurcations, and Chaos*, volume 8, pages 305–315. AMS, 1987.

[2] J. Bélair and M. Mackey. A model for the regulation of mammalian platelet production. *Ann. N. Y. Acad. Sci.*, 1:1–3, 1987.

[3] J. Bélair and M. Mackey. Consumer memory and price fluctuations in commodity markets: An integrodifferential model. *J. Dyn. and Diff. Eqns.*, 3:299–325, 1989.

[4] R. Braddock and P. van den Driessche. A population model with two time delays. *Math. Sci.*, 5:55–66, 1980.

[5] R. Braddock and P. van den Driessche. On a two lag differential delay equation. *J. Austral. Math. Soc.*, 24:292–317, 1983.

[6] K. Cooke and P. van den Driessche. On zeroes of some transcendental equations. *Funckcialaj Ekvacioj*, 29:77–90, 1986.

[7] L. E. El'sgol'ts (translated by R. J. McLaughlin). *Introduction to the Theory of Differential Equations with Deviating Arguments.* Holden-Day, Inc., San Francisco, CA, 1966.

[8] J. M. Ferreira and I. Györi. Oscillatory behavior in linear retarded functional differential equations. *J. Math. Anal. Appl.*, 128:332–346, 1987.

[9] J. Hale, E. Infante, and P. Tsen. Stability in linear delay equations. *J. Math. Anal. Appl.*, 105:533–555, 1985.

[10] J. K. Hale. *Theory of Functional Differential Equations.* Springer-Verlag, New York, 1977.

[11] J. K. Hale and W. Huang. Global geometry of the stable regions for two delay differential equations. Preprint 1991.

[12] N. Hayes. Roots of the transcendental equation associated with a certain differential difference equation. *J. London Math. Soc.*, 25:226–232, 1950.

[13] T. D. Howroyd and A. M. Russell. Cournot oligopoly models with time lags. *J. Math. Econ.*, 13:97–103, 1984.

[14] G. Ladas and I. P. Stavroulakis. Oscillations caused by several retarded and advanced arguments. *J. Diff. Eq.*, 44:132–152, 1982.

[15] M. C. Mackey. Commodity price fluctuations: Price dependent delays and nonlinearities as explanatory factors. *J. Econ. Theory*, 48:497–509, 1989.

[16] C. Marriott, R. Valleé, and C. Delisle. Analysis of a first order differential-delay equation containing two delays. *Physical Review A*, 40(6):3420–3428, 1989.

[17] R. D. Nussbaum. Differential delay equations with two time lags. *Mem. Amer. Math. Soc.*, 16:1–62, 1975.

[18] J. Ruiz-Claeyssen. Effects of delays on functional differential equations. *J. Diff. Eq.*, 20:404–440, 1976.

[19] E. Zaron. The delay differential equation: $x'(t) = -ax(t) + bx(t-\tau_1) + cx(t-\tau_2)$. Technical report, Harvey Mudd College, Claremont, CA, 1987.